Hindawi
Advances in Materials Science and Engineering
Volume 2020, Article ID 4326208, 22 pages
https://doi.org/10.1155/2020/4326208

Research Article

Study on Seismic Performance of Improved High-Strength Concrete Pipe-Pile Cap Connection

Zhijian Yang,[1] **Guochang Li**,[1] **and Bo Nan**[2]

[1]*School of Civil Engineering, Shenyang Jianzhu University, Shenyang 110168, China*
[2]*College of Water Conservacy, Shenyang Agricultural University, Shenyang 110866, China*

Correspondence should be addressed to Bo Nan; nb2003ccc@163.com

Received 8 March 2020; Revised 24 May 2020; Accepted 2 June 2020; Published 26 July 2020

Academic Editor: Antonio Caggiano

Four prestressed high-strength concrete pile- (PHC pile-) pile cap connections under low-cycle loading were tested to study the test phenomena, failure modes, hysteretic performance, ductility, and bearing capacity. The PHC piles were reinforced with steel fiber and deformed bars and CFRP. The tests results showed that the connections were damaged by bending. The concrete of the caps were squeezed to be crushed. The concrete of connection was crushed and formed a hinge joint that resulted in the connection rotating unrestricted, and the rotation capacity of connection increased. The PHC pile reinforced with steel fiber and deformed bars can improve the displacement ductility of the connections. The finite element software ABAQUS was used to simulate the nonlinear behavior of pile-cap connections. The prediction agreed relatively well with the experimental results. The stress and strain of specimens were studied. The connections should be designed with enough rotating capacity and make sure the cap will not be damaged by squeezing or prying due to the rotation of pile end.

1. Introduction

Prestressed high-strength concrete piles (PHC piles) have the advantages of low cost, high bearing capacity, high concrete strength, quick speed of construction, and good reliability; PHC piles have been widely used in Asian countries, such as Japan, China, and South Korea, and more than two hundred million meters of PHC piles are applied in engineering every year in China. The pile foundation needs to undertake the vertical load of the upper structure and horizontal force when subjected to earthquake. As the flexural bearing capacity of the pile is insufficient or the deformation capacity is poor, the different degree of damage may occur. Japan is one of the most vulnerable nations to earthquakes in the world; the investigation of previous earthquakes in Japan showed that the PHC pile to pile cap connection was damaged in earthquake, and the main failure modes are flexural and shear destruction [1–5].

In order to improve the horizontal bearing capacity of PHC piles, a lot of research has been done. Kokusho et al. [6, 7] found that a combination of concrete filled in the hollow part of PHC piles and high-strength spiral hoop was very effective for improving the deformability of PHC piles. Nagae et al. [8, 9] conducted cyclic test on prestressed reinforced concrete pile (PRC pile) and considered the effect of axial deformed bars and lateral reinforcement on the seismic performance of PRC piles. The test result showed that PRC piles can exhibit stable hysteretic behavior and significant ductility when properly reinforced with axial deformed bars and lateral reinforcement. The test result of Akiyama et al. [10] showed that the prestressed reinforced concrete pile with carbon-fiber sheets and infilled concrete had a much higher flexural bearing capacity than conventional precast concrete pile. Hyun et al. [11] showed that the shear strength of PHC pile could be increased by means of shear reinforcement and infilled concrete. Bang et al. [12] found that the maximum bending moment of the PHC pile improved with infilled concrete, and transverse and longitudinal reinforcement was approximately 45% higher than PHC pile. Yang et al. [13–15] conducted cyclic tests and finite element analysis to study the parameters of different types of pile, stirrup ratio, filling-concrete, steel fiber, and

deformed steel bar on the seismic performance of PHC pile. The test results showed that the PHC piles were damaged by bending. The bearing capacity and ductility of PHC pile increased with the reinforcement ratio of prestressing tendon. Concrete-filled in the hollow section could improve the bearing capacity and hysteretic performance of the PHC pile. Steel fiber had little effect on the performance of the PHC pile. The hysteretic loops of PHC pile reinforced with deformed steel bar were plumper, and the energy dissipation was good. Li et al. [16] studied the performance of CFST columns with foundation and columns without foundation. Zhang et al. [17] conducted tests of six full-scale prestressed high-strength concrete piles under combined axial compression and cyclic horizontal loads, and different axial compression levels and prestressing levels of prestressed tendons were studied. Test results indicated that the axial compression ratio and prestressing level of prestressed tendon significantly influenced the seismic performance of prestressed high-strength concrete piles. Wu et al. [18, 19] developed prestressed high-strength concrete (PHC) piles reinforced with high-strength materials (glass fiber-reinforced polymer (GFRP) bars) for flexural performance enhancement.

The performance of connection between pile and cap determined whether the upper structure and foundation can work together effectively. Based on the earthquake investigation of Japan [3, 4], the force of pile and cap connection was complicated and even simultaneously sustained the action of bending, shear, and axial load, which made the connection easy to be damaged.

Wachi et al. [20] proposed a simplified pile-to-pile cap connection for PHC pile; the test results showed that the degree of restraint against rotation of simplified connection is about 0.7 times the usual connection under stationary axial load condition, and the simplified connection has adequate shear strength under the condition without pull force. Aoshima et al. [21, 22] proposed an improved simplified connection with a tapered clearance around the pile head. The test results indicated that the simplified connection is very useful to reduce the bending moment of the pile head.

Hirade et al. [23] proposed a pile head joint method for prestressed high-strength concrete piles using unbonded stud bars; it found that the proposed joint method has high rotation performance which will decrease damage of piles. Sasaki et al. [24] used unbonded round steel bars with anchor plates to improve the performance of semirigid connections on pile heads by reducing the stress on pile heads and decreasing the cost of foundation works. It showed that the connection developed retains its bending capacity at rotational angles of less than 1/20 radian. Therefore, the behavior of anchor bars influences the performance of pile to cap connection. The slip between cap concrete and anchor bars may be beneficial to the rotation of pile end and may decrease the damage of pile end.

Many research studies have been carried out in South Korea. Park et al. [25] suggested a newly optimized method of reinforcing joint of PHC pile and foundation plate, and the test results indicated that the reduction of rebar reinforcement compared to previous method would lead to cost saving in PHC pile construction. Bang et al. [26] investigated the cyclic behavior and performance of the concrete infilled composite PHC (ICP) pile-footing connection; it indicated that the ICP pile-footing connection exhibited higher seismic and connection performance than the conventional PHC pile-footing connection. Bang et al. [27] provided an experimental and analytical study on the reinforced large diameter pretensioned high-strength concrete pile which was reinforced with infilled concrete, longitudinal rebar, and transverse rebar to increase the flexural and shear strength of conventional large-diameter PHC pile.

Researchers in China also have conducted some research studies on bending performance of PHC pile to pile cap under cyclic loading. Wang et al. and Yang and Wang [28, 29] studied six PHC pile-pile cap connections under cyclic loading; the test result showed that the specimens exhibit flexural failure, and the bearing capacity and energy dissipation capacity increased along with the rotation capacity of the pile connections. Guo et al. [30] studied the pile-cap connection of PHC pile considering two improved connection; the test results showed that the three connections experience different failure patterns. Blandon et al. [31] conducted cyclic test on two precast pretensioned pile-deck connections used in the construction of pile-supported marginal wharfs which were tested under cyclic loading.

The above studies indicate that many research studies have been done to improve the performance of PHC piles and the pile-pile cap connection, but the study about the performance of improved PHC pile-pile cap connection is relatively rare. To avoid the damage of end of PHC near pile-pile cap connection, three improved PHC pile-pile cap connections were studied by test and finite element analysis.

2. Experimental Program

2.1. Specimen Design. Four full-scale specimens were designed; the connections between pile and cap were same, as shown in Figure 1. The number of anchor bars should be not less than six to transfer forces from pile to cap according to Technical Code for Building Pile Foundation (JGJ 94–2008) of China [32]. The thickness of anchor plate is 20 mm, and the steel grade is Q235. Different methods were considered to improve the performance of the connections, such as reinforced with steel bars, steel fiber-reinforced, and CFRP (carbon fiber-reinforced polymer). CT-7 specimen was normal specimen with no improvement, the pile of CT-8 specimen was confined by three layers of CFRP, steel fiber was added into the pile of CT-9 specimen, and the pile of CT-10 specimen was reinforced with deformed bars. Table 1 summarizes the details of the specimens.

The diameter and thickness of the piles are 500 mm and 100 mm, respectively. The length of the pile is 2 m, and it is embedded into cap for 100 mm, as shown in Figure 1(a). Eleven 9.0 mm diameter of prestressing bars with an applied prestress of 994 MPa (70% gross ultimate tensile strength) were used. The stirrup spacing and diameter were 80 mm and 5 mm, respectively. An $1800 \times 1100 \times 850$ mm cap

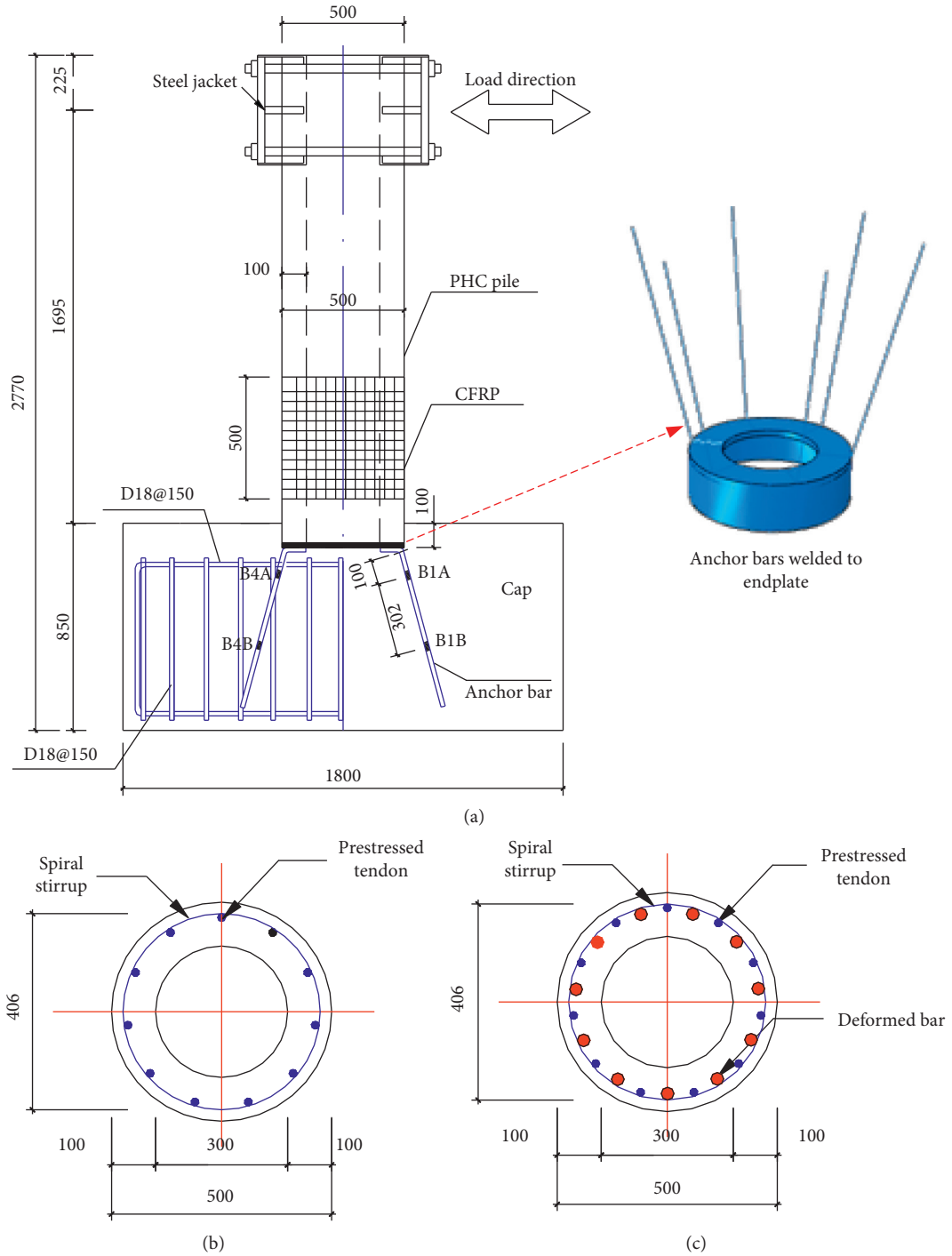

Figure 1: Details of specimens. (a) The connection between cap and pile. (b) PHC pile section. (c) PRC pile section.

Table 1: Parameters of specimens.

Specimen	D (mm)	t (mm)	Prestressing bars	Stirrup	Anchor bars	Improved measure of PHC pile
CT-7	500	100	11**A**9.0	**A**5@80	6B18	—
CT-8	500	100	11A9.0	A5@80	6B18	Three layers of CFRP
CT-9	500	100	11A9.0	A5@80	6B18	Volume fiber content 1.0%
CT-10	500	100	11A9.0	A5@80	6B18	11**B**14

Note. D is the diameter of PHC pile and t is the thickness of PHC pile.

section was used, and Figure 1(a) shows reinforcement used for specimens. The cross sections of PHC pile PRC pile are shown in Figure 1(c). Six anchor bars were welded to the anchor plate and then bent outward into the cap in a 75° pattern, as shown in Figure 1(b).

2.2. Specimen Preparation. PHC piles were fabricated with centrifugation, steam, and autoclave curing at factories. PHC piles were steamed at atmospheric pressure for 6 hours at 80°C and steamed at high temperature and pressure for 6–8 hours (1.0 MPa, 180°C). The cap was naturally cured. Because the scale of cap is large, it was not convenient to fabricate them as actual engineering; therefore, the concrete of cap was cast by convert. Microexpensive concrete was cast into both the hollow section of pile and cap simultaneously. Deformed bars are arranged at intervals in PRC pile, as shown in Figure 1(c). The optimal amount of steel fiber was determined according to the study results of [33–35]. The hooked steel fiber (as shown in Figure 2) was used to improve PHC pile; the equivalent diameter, average length, and the ultimate tensile strength are 0.5 mm, 32 mm, and 1000 MPa, respectively. To improve the dispersion uniformity of steel fiber in the mixing materials, the method of dry mixing and wet mixing was adopted. When preparing the specimen CT-8, the surface of pile was made to be rough, and then the CFRP sheet was wrapped around the pile, as shown in Figure 3. The CFRP sheet was wrapped with three layers with a 150 mm overlap in the direction of fibers to ensure proper bond.

2.3. Material Properties. The mechanical properties of steel bars are listed in Table 2. The concrete proportioning of PHC pile and cap is listed in Table 3. The concrete compression strength of pile and cap is shown in Table 4. Tensile tests on CFRP coupons were conducted according to the Chinese standard GB/T 3354-1999 [36]. The values presented were the averages from three test coupons based on a nominal thickness of 0.167 mm/ply. The ultimate tensile strength is 3718 MPa, elastic modulus is 2.75 × 106 MPa, the ultimate strain is 0.13678, and the Poisson ratio is 0.304.

2.4. Loading Device. The test setup is shown in Figure 4. The cap was anchored to the strong floor firstly before the axial load and cyclic lateral load were applied on the pile, where "1" is an actuator with 600 kN capacity and push/pull stroke of 300 mm, "2" and "5" are load sensors, "3" is counterforce frame, "4" is sliding plate, "6" is a 1000 kN hydraulic jack, "7" is PHC pile, "8" is inclinometer, and A1~A8 are displacement sensors. Four displacement sensors were placed on one side of the pile at 420 mm spacing from the pile base to monitor the lateral displacements. Rotation of the pile was monitored using two 50 mm range displacement sensors placed on the two sides of the column in the loading plane. The axial load was applied by a 1000 kN hydraulic jack.

2.5. Loading Schedule. The loading protocol is very important and strongly influences the test results [37, 38], the test was performed with load and displacement mix control according to the Specification for Seismic Test of Buildings JGJ/T101-2015 [39], and the load program is shown in Figure 5. The axial load about 500 kN was firstly applied, which must be kept constant during loading. The yield load was defined as the anchor bar researched its yield strain, and the corresponding displacement was defined as yield displacement.

The load control was used before the yield of specimen, and one cycle was applied at each of the elastic lateral load. The subsequent load cycles were displacement controlled and consisted of three cycles after the specimen yielded. Test was terminated due to large deformation or when the bearing capacity of specimen had deteriorated to 85% of the maximum load. Two strain gauges were pasted on every anchor bar, and the length of the strain gauge is 3 mm, as shown in Figure 1(a). To measure the concrete strain of pile, eight strain gauges were arranged at 200 mm from the pile base; the length of the strain gauge is 80 mm, as shown in

Figure 2: The hooked steel fiber.

Figure 3: Wrapping CFRP sheet.

Table 2: Material properties of steel.

Steel	d (mm)	f_y (MPa)	f_u (MPa)	E_s (MPa)
Prestressing tendon	**A**9.0	—	1560	2.0×10^5
Deformed steel bars	**B**14	403	600	2.0×10^5
	B18	352	583	2.0×10^5
Stirrup	**A**5	—	601	2.0×10^5

Note. d is the diameter of the steel bar, f_y is the yield strength, f_u is the ultimate strength, and E_s is the elastic modulus.

Table 3: Concrete proportioning of PHC pile and cap (kg/m^3).

Materials	Cement	Mineral admixture	Sand	Stone	Compound admixture	Water
Pile	336	144	639	1187	9.6	139
Cap	476	0	556	1183	0	195

Table 4: Concrete compressive strength.

Concrete	No. 1 (MPa)	No. 2 (MPa)	No. 3 (MPa)	No. 4 (MPa)	No. 5 (MPa)	Mean (MPa)
Normal pile	74.9	84.2	88.4	89.3	89.1	85.2
Volume fiber content 1.0%	88.1	89.5	82.1	87.6	88.9	87.2
CAP of CT-7	45.7	32.9	64	58.9	37.8	47.9
CAP of CT-8	49.9	46.9	45.6	47.9	47.5	47.5
CAP of CT-8	56.4	32.9	50.6	56.9	57.0	50.8
CAP of CT-10	57.0	50.1	55.6	58.3	57.0	55.6

Note. The concrete strength of normal pile contains the specimens CT-7, CT-8, and CT-10, volume fiber content 1.0% refers to the concrete strength of pile in CT-9, and CAP of CT-7 refers to the concrete strength of cap in CT-7.

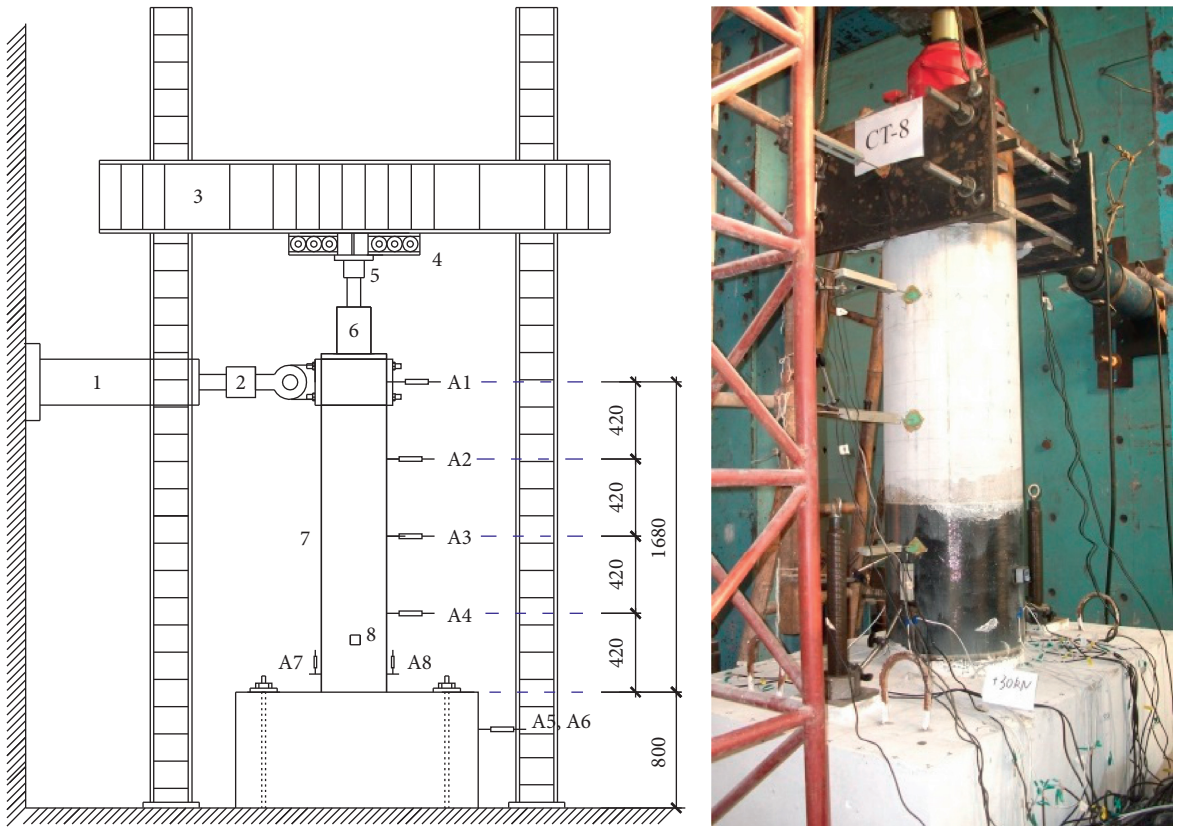

Figure 4: Test setup. (a) Diagrammatic test setup. (b) Test photo.

Figure 6(a). Eight strain gauges were attached on CFRP; the length of the strain gauge is 5 mm, as shown in Figure 6(b).

3. Test Observations

For Specimen CT-7, as the loads were 120 kN and −150 kN, crack appeared at the tensile pile hoop and pile body interface. At the Δ_y displacement ($\Delta_y = 6$ mm), a 0.05 mm wide circumferential crack appeared at the tensile region of pile which was 450 mm apart from top of cap. At the $2\Delta_y$ displacement, a 0.05 mm wide circumferential crack appeared at the tensile region of pile which was 350 mm apart from top of cap. At the $3\Delta_y$ displacement, multiple radial cracks appeared on the tensile region of cap, the maximum crack width was 0.2 mm, and a crack extended to the compressive region and side of the cap. The width of crack between the tensile pile hoop and pile body interface was 1.7 mm. At the $4\Delta_y$ displacement, all the cracks of cap had extended, and the

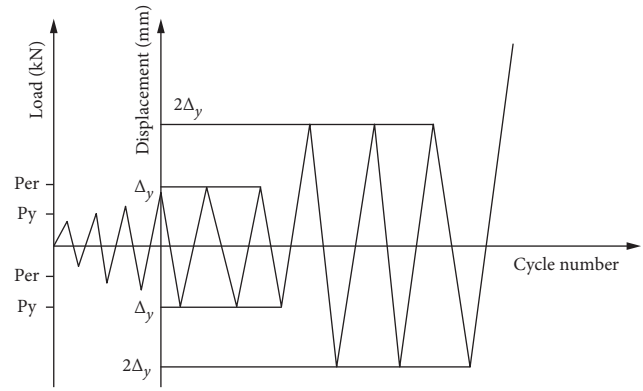

Figure 5: Load program.

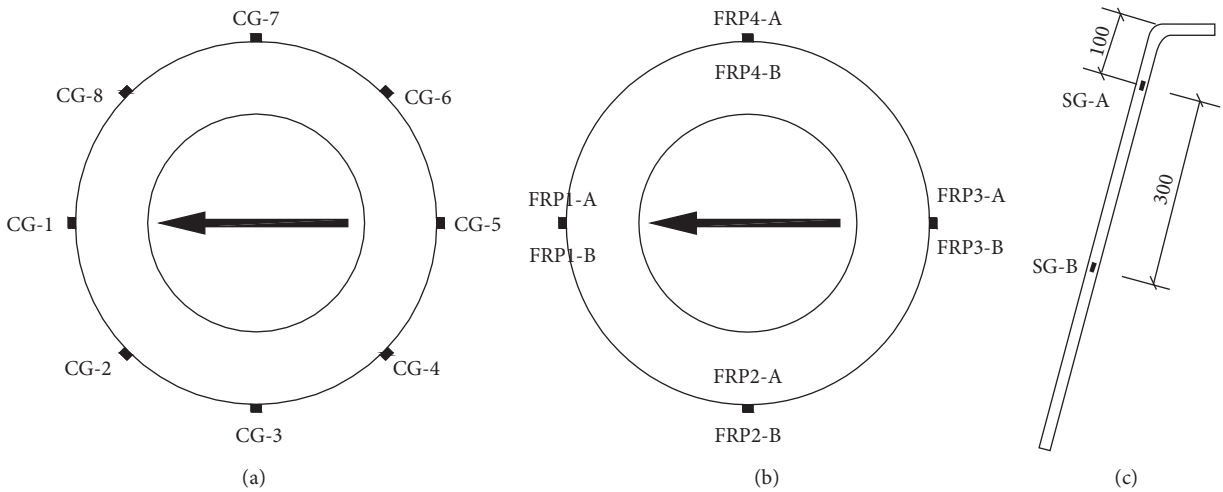

Figure 6: Location of strain gauges. (a) Concrete. (b) CFRP. (c) Anchor bar.

maximum width of crack was 0.9 mm. A 1 mm width gap occurred between the tensile area of pile and cap. The pile body had the tendency to be pulled out, and the cracks of pile did not develop any more. At the $5\Delta_y$ displacement, the cracks of cap extended, and the maximum width of crack was 1.8 mm. The gap between the tensile area of pile and cap was 2 mm, and the pile was pulled out about 2 mm from cap. At the $6\Delta_y$ displacement, the concrete of cap appeared uplift, the gap between the tensile pile and cap was 3 mm, and the maximum width of cap crack was 2 mm. The failure mode of CT-7 is shown in Figure 7(a).

For Specimen CT-8, as the loads were 90 kN and −90 kN, cracks appeared at the tensile pile and cap. At the Δ_y displacement ($\Delta_y = 6.5$ mm), a 0.1 mm wide crack appeared at the tensile pile hoop and pile body interface. At the $2\Delta_y$ displacement, the crack between the tensile pile hoop and pile body interface was 0.8 mm. At the $3\Delta_y$ displacement, the cap appeared uplift, the gap between the tensile pile and cap was 0.65 mm, and the crack between the tensile pile hoop and pile body interface was 1.2 mm. At the $-3\Delta_y$ displacement, multiple radial cracks appeared on the tensile region of cap, and the maximum crack width was 0.45 mm. At the $-4\Delta_y$ displacement, the radial cracks of the cap extended, and a crack about 500 mm long appeared along the side of the cap. At the $5\Delta_y$ displacement, the uplift of cap was obvious, and the maximum crack width was 0.65 mm. At the $6\Delta_y$ displacement, the concrete cover of cap at tensile side tended to spall, and cracks appeared along two sides of the cap of long side direction, which were about 1.2 m in length and 1 mm in width. The failure mode of CT-8 is shown in Figure 7(b).

For Specimen CT-9, as the loads were 120 kN, cracks appeared at the tensile pile and cap. At the $2\Delta_y$ displacement ($\Delta_y = 6$ mm), a 0.1 mm wide circumferential crack appeared at the tensile region of pile which was 350 mm apart from top of cap. The tensile region of cap appeared uplift, and the width of crack was 0.1 mm. At the $-2\Delta_y$ displacement, crack appeared at the tensile pile hoop and pile body interface, and a 0.05 mm wide circumferential crack appeared at the tensile region of pile which was 250 mm apart from top of cap. At the $3\Delta_y$ displacement, a 0.05 mm wide circumferential crack appeared at the tensile region of pile which was 550 mm apart from top of cap, and the width of crack between the tensile pile hoop and pile body interface was 1.1 mm. At the $-3\Delta_y$ displacement, a 0.05 mm wide circumferential crack appeared at the tensile region of pile which was 500 mm apart from top of cap. At the $-4\Delta_y$ displacement, the uplift of concrete cover of cap was obvious. At the $8\Delta_y$ displacement,

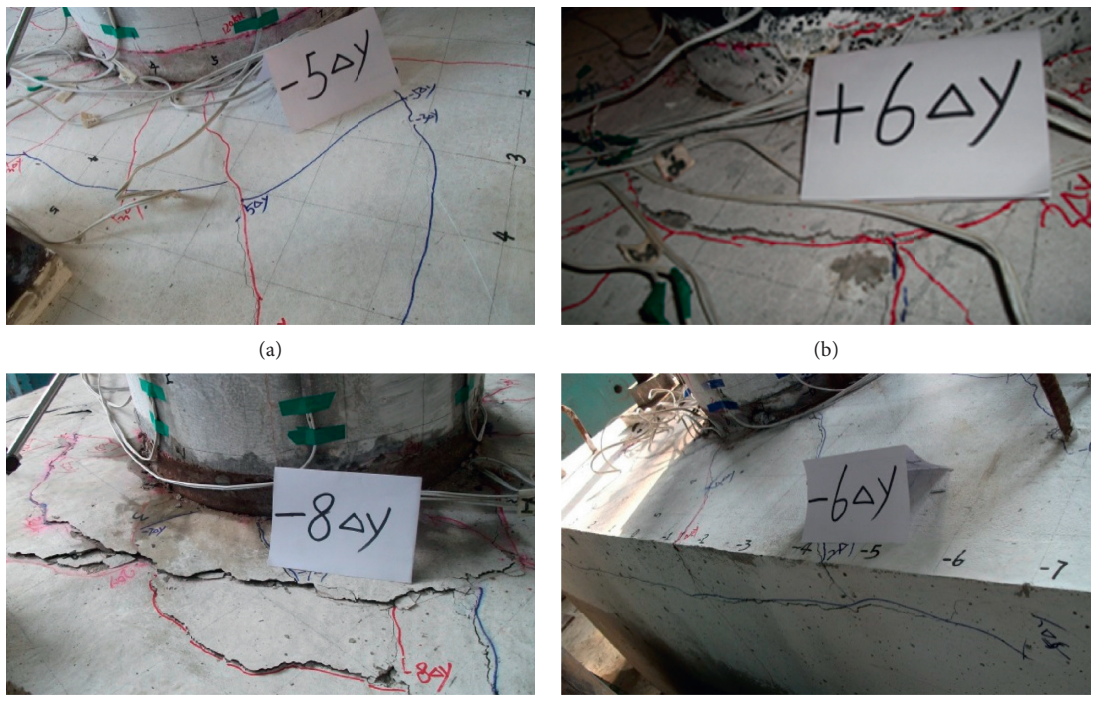

Figure 7: Failure mode of specimens. (a) CT-7. (b) CT-8. (c) CT-9. (d) CT-10.

the concrete cover of cap at tensile side tended to spall, the gap between pile and cap was 4 mm, and the pile was pulled out about 8 mm. The failure mode of CT-9 is shown in Figure 7(c).

For Specimen CT-10, as the loads were 120 kN, cracks appeared at the tensile pile and cap. At the Δ_y displacement ($\Delta_y = 6.5$ mm), a crack appeared at the tensile pile hoop and pile body interface, and the width is 0.05 mm. At the $2\Delta_y$ displacement, two circumferential cracks appeared at the tensile region of pile, which were 150 mm and 320 mm apart from top of cap, respectively. At the $-2\Delta_y$ displacement, a 0.08 mm wide circumferential crack appeared at the tensile region of pile which was 250 mm apart from top of cap. At the $3\Delta_y$ displacement, multiple radial cracks appeared on the tensile region of cap, and the maximum crack width was 1.1 mm. A 0.08 mm wide circumferential crack appeared at the tensile region of pile which was 580 mm apart from top of cap. The crack width of 150 mm and 320 mm apart from top of cap was 0.25 mm. At the $5\Delta_y$ displacement, a crack appeared along long side of the cap, which was about 0.7 m in length and 1.5 mm in width. At the $6\Delta_y$ displacement, there was an overall uplift trend at the tensile region of cap, the pile has the sign to be pulled out, and the maximum crack width of the cap was 2 mm. At the $-6\Delta_y$ displacement, the cap had a large-scale uplift, and the specimen could no longer bear the load. The failure mode of CT-10 is shown in Figure 7(d).

4. Test Result and Discussion

4.1. Load-Displacement Hysteretic Curves. Load-displacement hysteretic curves of specimens are shown in Figure 8. The failure of specimen CT-7~CT-10 was due to the crushing of cap concrete and slip of anchor bars, which caused the connection to be hinge joint. The hysteretic performance of pile-cap connection was mainly determined by the cap and anchor bars; therefore, the hysteretic curve pinched seriously. After $3\Delta_y$ displacement, the bearing capacity of specimen CT-7 decreased with the increase of displacement because of the yield of anchor bars. Specimen CT-8 was reinforced by CFRP; it can be seen that the load increases with the increase of displacement. After $2\Delta_y$ displacement, the positive load does not increase, but the reversed load still increases. Specimen CT-9 was reinforced by steel fiber; because the cap of joint region was damaged, the improved effect to the seismic performance of connection is not obvious. Specimen CT-10 was reinforced by deformed bars, and the bearing capacity declined suddenly due to the rupture of anchor bar. The improvement of CFRP confine, reinforced with steel fiber and deformed bars, could increase the bearing capacity of pile end; otherwise, it made the joint region easy to be damaged. Therefore, the joint region should own enough rotation capacity to make sure the connection will not fail as the rotation is small, and the pile can take advantage of its flexural bearing capacity.

4.2. Strain Analysis. Figure 9 shows the concrete strain of CG-1 and CG-5. It can be seen that the maximum compressive strain of concrete is $-1780\,\mu\varepsilon$ which does not reach the ultimate compressive strain of concrete, and the concrete of pile was not crushed. The strain of CG-1 in CT-10 is $1500\,\mu\varepsilon$, which is different from CT-7~CT-9; because a crack appeared at the position of CG-1, the strain gauge was tensioned to be ruptured.

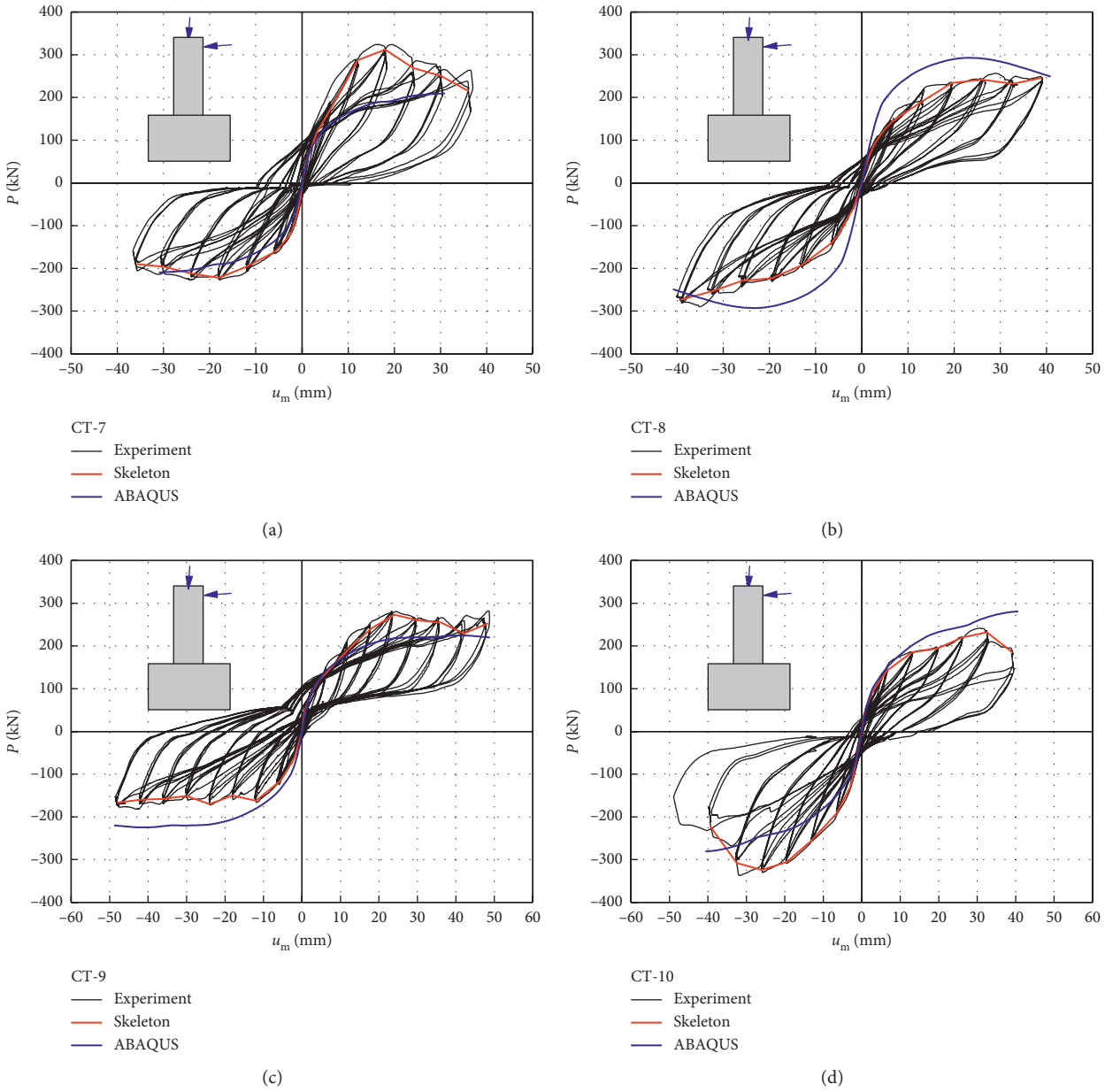

Figure 8: Hysteretic load-displacement response for specimens. (a) CT-7. (b) CT-8. (c) CT-9. (d) CT-10.

Figure 10 shows the load-strain curves of anchor bars; point A is the position of maximum stress. It shows that the strains of the specimen CT-7~CT-9 are smaller than 2000 $\mu\varepsilon$, which indicates that the anchor bars below the point did not yield.

Figure 11 shows the load-strain curves of CFRP, where FRP1-A and FRP1-B are the longitudinal strain and transverse strain, respectively. The maximum strain of FRP1-A is −1505 $\mu\varepsilon$ which is close to the concrete strain of CG-1, which indicates that the bond between CFRP and pile is good. The maximum strain of FRP1-B is 400 $\mu\varepsilon$; it means that the CFRP confined the concrete, but the effect is not obvious because the failure of CT-8 mainly focused on joint between pile and cap. The circumferential tensile stress of CFRP was small; therefore, the CFRP did not rupture or exhibit failure of overlap.

4.3. Bearing Capacity and Displacement Ductility. Displacement ductility factor is an important index to evaluate the behavior of structure under earthquake, which is defined as the ratio between ultimate displacement and yield displacement as follows:

$$\mu = \frac{\Delta u}{\Delta y}, \tag{1}$$

where Δu and Δy are the ultimate displacement and yield displacement, respectively.

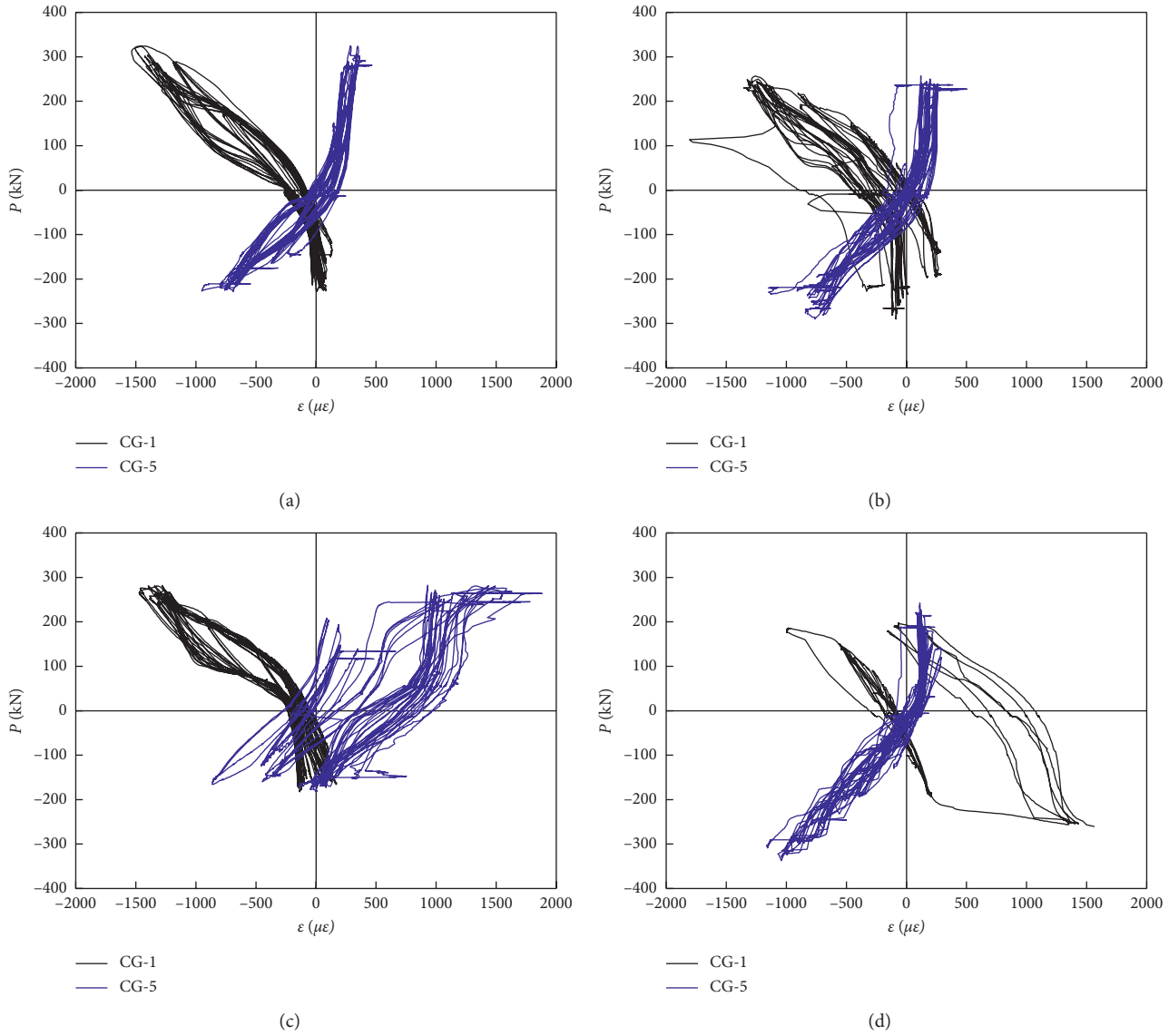

Figure 9: Load-stress curves of pile concrete. (a) CT-7. (b) CT-8. (c) CT-9. (d) CT-10.

The displacement corresponding to 85% of the maximum load is defined as Δu. When the bearing capacity does not decline or is less than 85% of the lateral bearing capacity, the corresponding displacement is taken as ultimate displacement. The yield displacement is determined according to energy method according to the Specification for Seismic Test of Buildings JGJ/T101-2015 [39]. The load-displacement skeleton curves of CT-7~CT-10 are shown in Figure 12. The displacement ductility factors, cracking moment (M_{cr}), and ultimate bending moment (M_u) are listed in Table 5; the cracking moment is the moment when the crack appears between pile and steel hoop.

It can be seen from Figure 12 and Table 5 that the bearing capacity and stiffness of the connections have not been increased after improvement, but the skeleton curves are more flat at the later stage of the loading. The average displacement ductility factors of CT-7~CT-10 are 2.42, 2.32, 3.52, and 2.51, respectively. The displacement ductility factors of CT-9~CT-10 are bigger, and the maximum value is 4.49. It indicates that the ductility of connection can be improved as the pile is reinforced with steel fiber and deformed bars. This is because after adding steel fiber, the compressive strength and tensile strength of concrete are increased, and the deformability can be improved. After the configuration of deformed bars, the flexural bearing capacity of the pile is increased. Yang et al. [13] conducted a test on PHC piles; the test results showed that the displacement ductility factors of PHC pile, PHC pile improved with steel fiber, and deformed steel bars are 2.39, 2.31, and 3.18, respectively. It indicates that the displacement ductility factors of CT-7~CT-10 specimens are larger than those of PHC pile so that the connection is viable in seismic areas.

4.4. Moment-Drift Angle of Pile Head. Figure 13 shows the moment-rotation relationship of pile head; the drift angle was recorded by an inclinometer. The curve of Figure 13 is

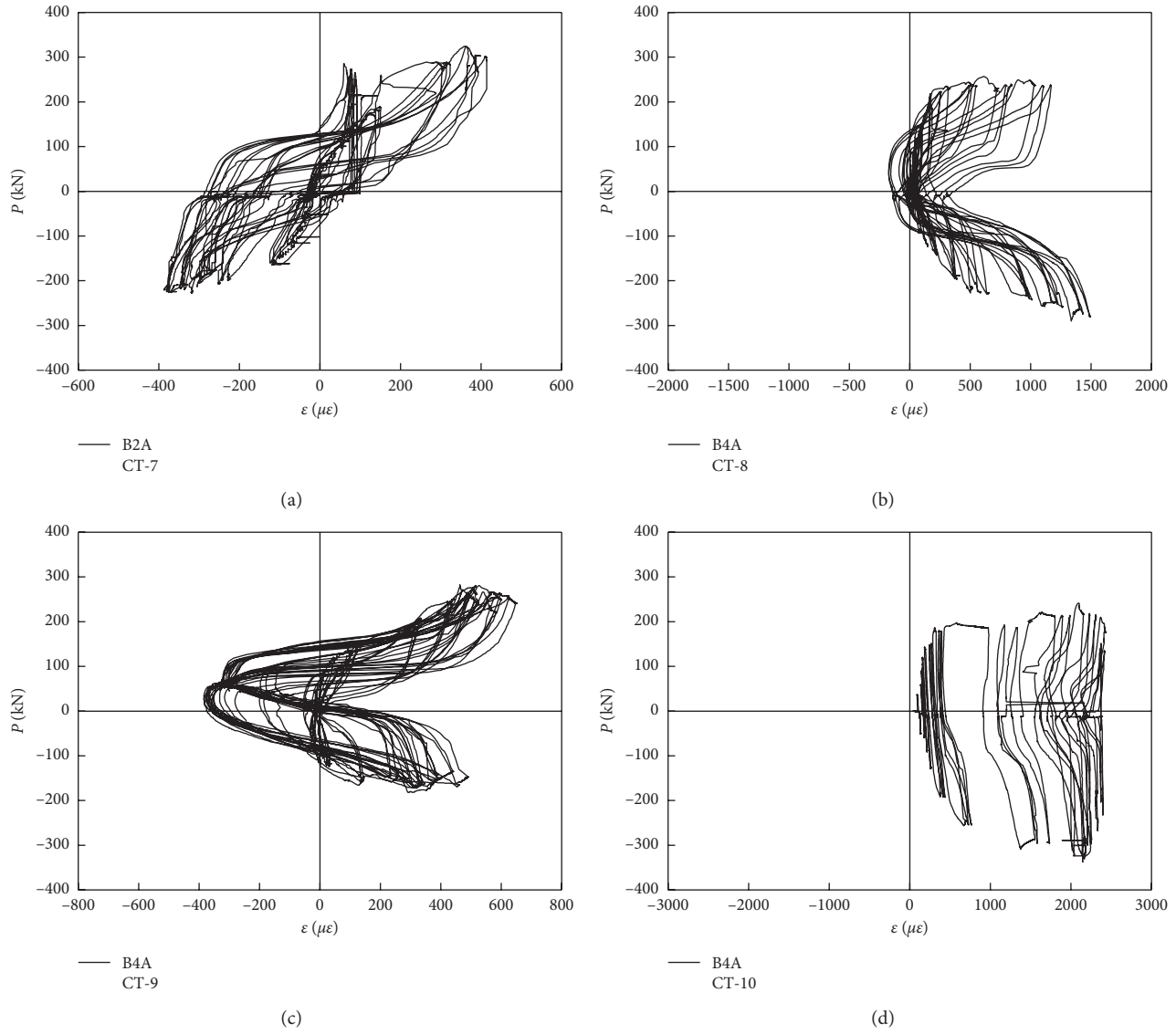

Figure 10: Load-strain curves of anchor bars. (a) CT-7. (b) CT-8. (c) CT-9. (d) CT-10.

similar to Figure 12, which means the drift angle is reliable. It can be seen from Figure 13 that the lateral load decreased with the increase of connection drift angle because the joint region of anchor bars lose restraint of concrete. In addition, as the connection drift angle was 0.014 rad, the concrete cover of cap spalled due to the prying and squeezing force of pile end. Plastic hinge formed at the connection between pile and cap and circumferential crack appeared at pile end, but the damage was not serious. In order to avoid the failure of cap under the prying and squeezing force of the pile end, the connection angle should be less than 0.014 rad.

4.5. Energy Dissipation. Damage states defined by Pagni and Lowes [40] have been used to evaluate the damage level of the structures; otherwise, the equivalent damping coefficient was used to evaluate the damage level and seismic performance of specimens. Figure 14 shows the equivalent damping coefficient of different displacement. It can be seen that the equivalent damping coefficient increases with the displacement. Before reaching $2\Delta_y$ displacement, the equivalent damping coefficient of the CT-7~CT-10 specimen has no obvious difference. At the process of loading to $3\Delta_y$ displacement, the cap of CT-8~CT-10 damaged more seriously than CT-7, the concrete of cap appeared uplift, and the restrain capacity of joint region weakened, which caused the equivalent damping coefficient of CT-8~CT-10 to be smaller than that of CT-7.

5. Finite Element Analysis

The experiment has studied the seismic behavior of improved PHC pile to cap connection so as to study the performance of the specimens further. The model of improved PHC pile to cap connection was established by the finite element analysis software ABAQUS; the load-displacement curve and the stress of longitudinal steel bars, anchor bars, and concrete were analyzed.

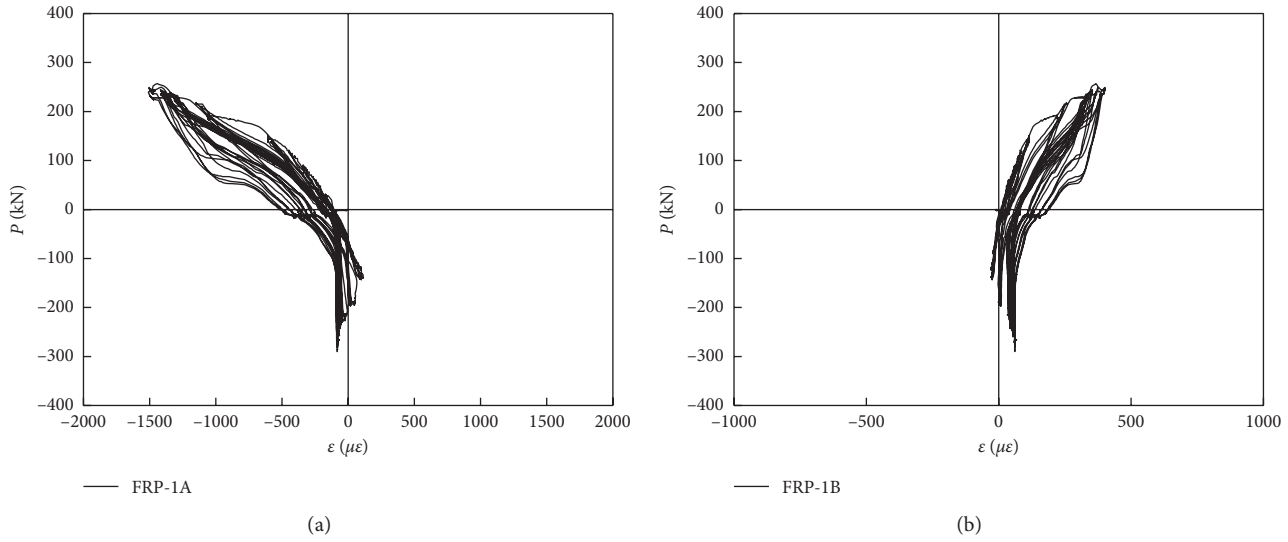

Figure 11: Load-strain curves of CFRP. (a) FRP1-A. (b) FRP1-B.

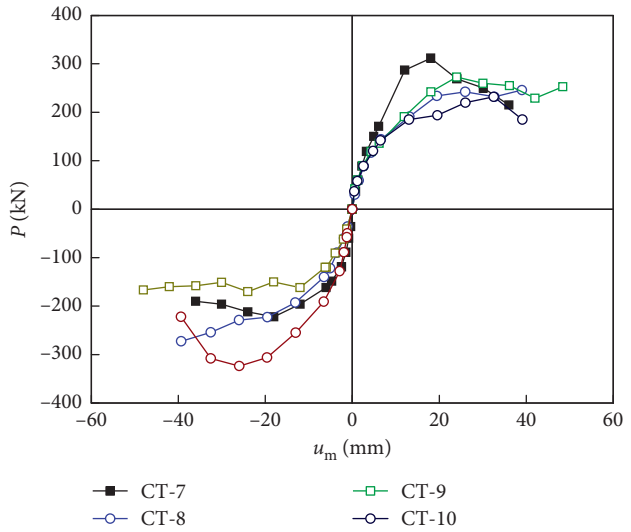

Figure 12: Load-displacement skeleton curves.

Table 5: Results of tests.

Specimen	M_{cr} (kN·m)		M_u (kN·m)		Δ_y (mm)		Δ_u (mm)		μ	
	Forward	Reverse	Forward	Reverse	Forward	Reverse	Forward	Reverse	Forward	Reverse
CT-7	208.3	−262.5	546	−388.5	11.8	−8.9	25.34	−24.02	2.15	2.70
CT-8	252	−248.5	430.5	−477.8	14.09	−21.1	39	−39.32	2.77	1.86
CT-9	238	−210	477.8	−297.5	16	−10.7	41.03	−48.02	2.56	4.49
CT-10	248.5	−334.3	406	−567	15.3	−14.5	39.13	−35.7	2.56	2.46

Note. M_{cr} is the cracking moment, M_u is the ultimate moment, Δ_y is the yielding displacement, Δ_u is the ultimate displacement, and μ is the displacement ductility factor.

5.1. Finite Element Model

5.1.1. Material Constitutive Model. The bilinear constitutive model of steel was used to simulate the steel. The concrete constitutive model used the concrete-damaged plasticity model in ABAQUS. The constitutive model proposed by Guo [41] was used to model the concrete which has been widely adopted as the uniaxial stress-strain curve for concrete in China. The compressive stress-strain relationship can be shown as follows:

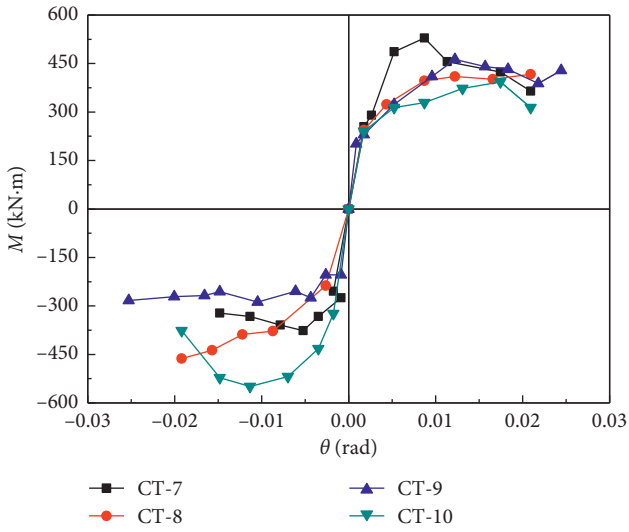

Figure 13: Moment-drift angle curves.

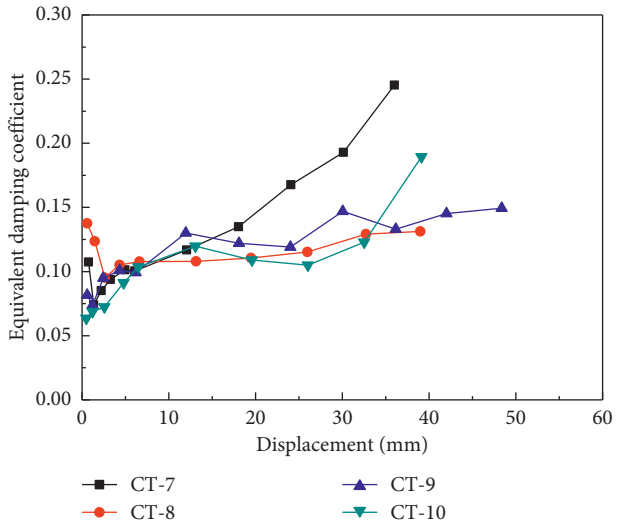

Figure 14: Equivalent damping coefficient.

$$\sigma = \begin{cases} f_c\left[\alpha_a\left(\frac{\varepsilon}{\varepsilon_c}\right) + (3-2\alpha_a)\left(\frac{\varepsilon}{\varepsilon_c}\right)^2 + (\alpha_a - 2)\left(\frac{\varepsilon}{\varepsilon_c}\right)^3\right], & (\varepsilon \le \varepsilon_c), \\ \dfrac{f_c \varepsilon}{\alpha_d (\varepsilon - \varepsilon_c)^2 + \varepsilon}, & (\varepsilon > \varepsilon_c), \end{cases} \tag{2}$$

where σ is the stress at strain ε, f_c is the axial compressive strength, and ε_c is the peak strain at stress f_c which can be calculated by equation (3), where α_a and α_d are constants. Equations (4) and (5) are used to estimate the constants α_a and α_d.

$$\varepsilon_c = \left(700 + 172\sqrt{f_c}\right) \times 10^{-6}, \tag{3}$$

$$\alpha_a = 2.4 - 0.0125 f_c, \tag{4}$$

$$\alpha_d = 0.157 f_c^{0.785} - 0.905. \tag{5}$$

The tension stress-strain relationship can be shown as follows:

$$\sigma = \begin{cases} f_t\left(1.2 - 0.2\left(\frac{\varepsilon}{\varepsilon_t}\right)\right), & (\varepsilon \le \varepsilon_t), \\ \dfrac{f_t \varepsilon}{\alpha_t \varepsilon_t^{0.3} (\varepsilon - \varepsilon_t)^{1.7} + \varepsilon}, & (\varepsilon > \varepsilon_t), \end{cases} \tag{6}$$

where f_t is the axial compressive strength and ε_t is the peak strain at stress f_t that can be calculated by equation (7). α_t is a constant, and equation (8) is used to estimate it.

$$\varepsilon_t = 65 f_t^{0.54} \times 10^{-6}, \tag{7}$$

$$\alpha_t = 0.312 f_t^2. \tag{8}$$

CFRP was assumed to be linear elastic. The fibers ruptured when researching the ultimate strain; therefore, the fibers could not take the load any more, as shown in the following equation:

$$\begin{aligned} &\varepsilon \le \varepsilon_f, \quad \sigma_f = E_f \varepsilon, \\ &\varepsilon > \varepsilon_f, \quad \sigma_f = 0, \end{aligned} \tag{9}$$

where σ_f is the ultimate stress of the fiber; E_f is the modulus of elasticity; and ε_f is the ultimate strain.

5.1.2. Element Type, Element Mesh, and Boundary Condition. Prestressing tendon and stirrup used T3D2 element, and C3D20R element was selected for concrete. CFRP used S4R element. The bond between filled concrete and inner wall of pile was assumed to be good; therefore, the two parts were tied to be together without considering the slip between them. "Hard contact" was used to simulate the contact of steel hoop and cap, endplate and cap, endplate and pile. The saddle and pile and steel hoop and pile were tied to be together, respectively. The prestressing tendon and stirrup were embedded into concrete, without considering the slip between concrete and bars. The prestress was applied with the decreasing temperature method. The CFRP and pile was tied to be together. Boundary conditions and mesh of the finite element analysis model are shown in Figure 15.

5.2. Model Verification. Finite element analysis (FEA) load-displacement curves under monotonic loading are compared with the experimental curves as shown in Figure 8. It can be seen that the FEA results are close to the experimental curves. Table 6 lists the FEA results. There are some certain errors between the FEA and test results about the bearing capacity and stiffness. The main reason is that the FEA could not simulate the action between steel head and endplate, so the prestressing stress was mainly transferred by bond between steel and concrete. Therefore, it would result in the increase of the transfer length of prestressing bar, and the effective prestressing stress of pile will be smaller than

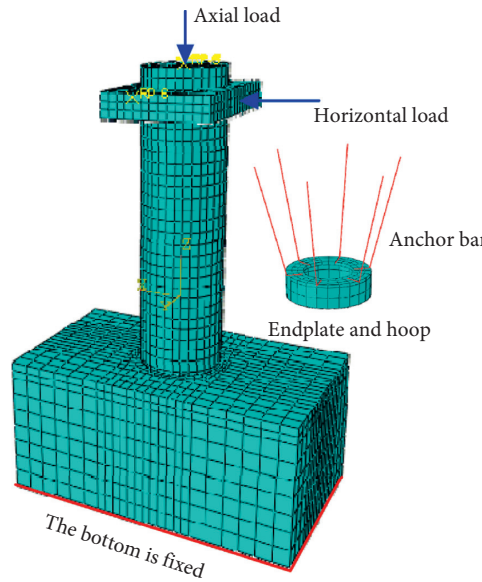

Figure 15: Finite element model.

Table 6: Comparisons between experimental and finite element analysis results.

Specimen	P_{Eu} (kN)		P_{Fu} (kN)		P_{Eu}/P_{Fu}	
	Forward	Reverse	Forward	Reverse	Forward	Reverse
CT-7	312	−215	218	−218	0.70	1.01
CT-8	246	−273	293	−293	1.19	1.07
CT-9	273	−170	225	−225	0.82	1.32
CT-10	232	−324	281	−281	1.21	0.87

Note. P_{Eu} is the experimental result and P_{Fu} is the finite element analysis result.

practical situation. In addition, the bearing capacity of the specimen will decrease continuously when it is cracked and closed under repeated loads, but this situation will not occur when the FEA is monotonously loaded, so the FEA result is basically larger than the test result. In addition, axial force of pile head cannot remain constant in the test, which makes the load and stiffness of two directions to be different. Otherwise, the axial load can remain unchanged in the process of calculation, and it also makes the FEA curve and test curve to have certain differences. Despite the influence of the above factors, the FEA results are not far from the test results, which can be used as a basis for further analysis.

5.3. Analysis of Stress

5.3.1. Stress Distribution of Steel Bars. Figures 16–19 show the stress distribution of steel bars of specimen CT-7~CT-10 at ultimate state.

Figure 16 shows the stress distribution of steel bars of specimen CT-7. The anchor bars yielded due to tension at the interface between and cap. The yield length is about 100 mm near the endplate. The closer the position is to the endplate, the greater the steel stress is, and yielding does not occur outside 100 mm. The maximum tensile stress of the stirrups is 544.9 MPa, but it does not reach the ultimate stress. Because the concrete was under compression, the stirrup restrained the lateral deformation of concrete, which caused it to bear high tensile stress. The maximum tensile stress of prestressing bars in the tensile zone is 1451 MPa, which has already yielded.

Figure 17 shows the stress distribution of steel bars of specimen CT-8. As can be seen from Figures 17(a)–17(c), the stress of anchor bar, stirrup, and prestressing bar is basically the same as that of CT-7 after reinforced with CFRP. The circumference tensile stress distribution of CFRP is shown in Figure 17(d). The maximum tensile stress of CFRP is 312 MPa, which appeared at the compressive zone. It indicates that CFRP confined the concrete, but the stress is small, which is close to the results of the test.

Figure 18 shows the stress distribution of steel bars of specimen CT-9. The maximum tensile stress of anchor bars is 1062 MPa, which is bigger than CT-7. The maximum tensile stress of prestressing bars is 1399 MPa, which is smaller than CT-7. Considering the effect of steel fiber in analysis, the ultimate tensile stress of concrete was increased, which caused the concrete to share a part of the tensile stress of the prestressing bars, and its tensile stress decreased.

Figure 19 shows the stress distribution of steel bars of specimen CT-10. The maximum tensile stress of anchor bars is 1386 MPa, which is bigger than its ultimate tensile strength. It can be seen from Figure 19(b) that the stress of

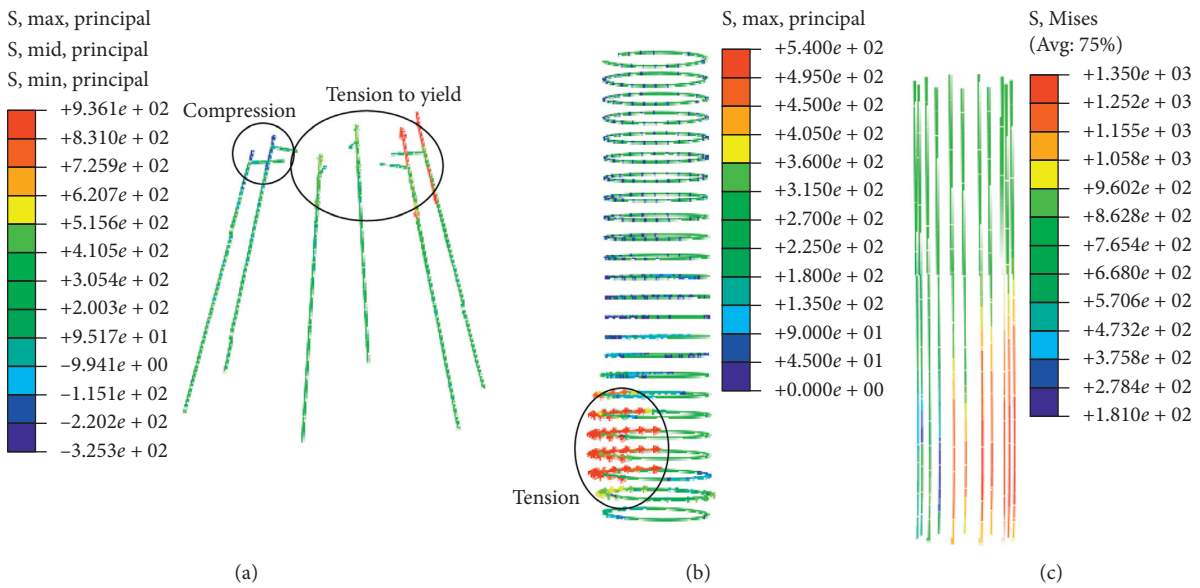

Figure 16: The stress distribution of specimen CT-7. (a) Anchor bars. (b) Stirrup. (c) Prestressed bar.

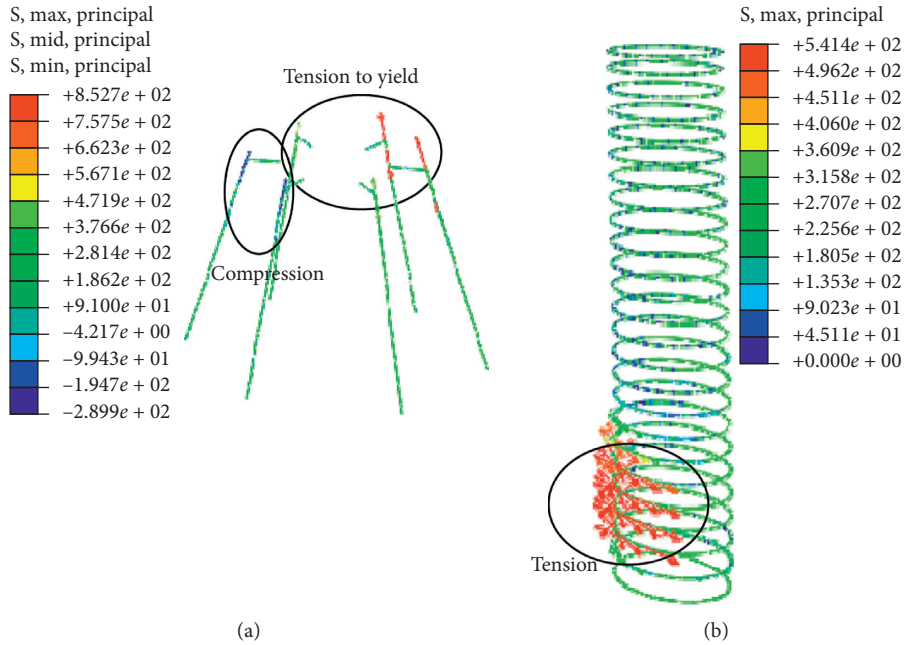

Figure 17: Continued.

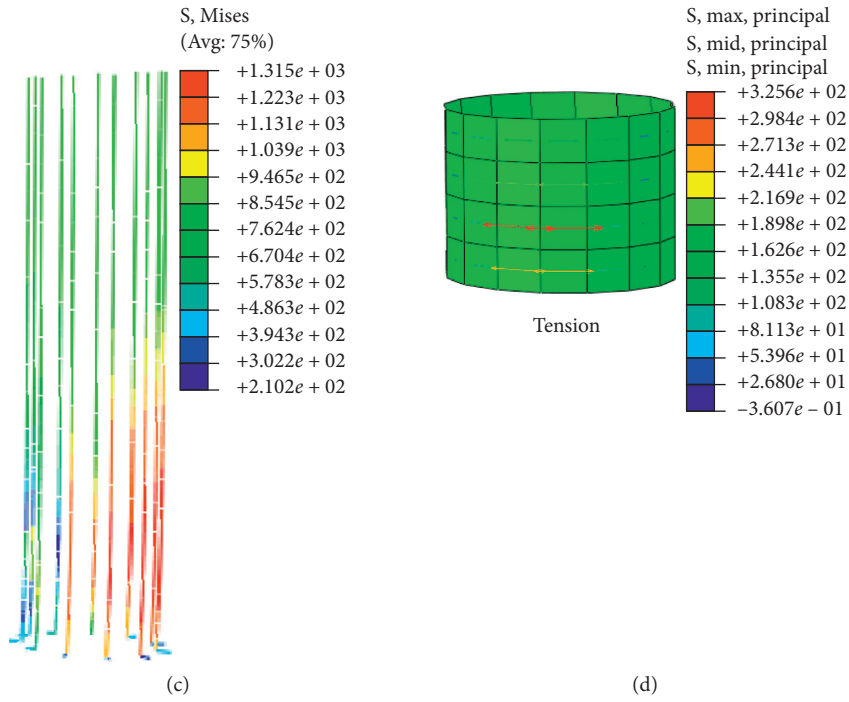

Figure 17: The stress distribution of specimen CT-8. (a) Anchor bars. (b) Stirrup. (c) Prestressed bar. (d) CFRP.

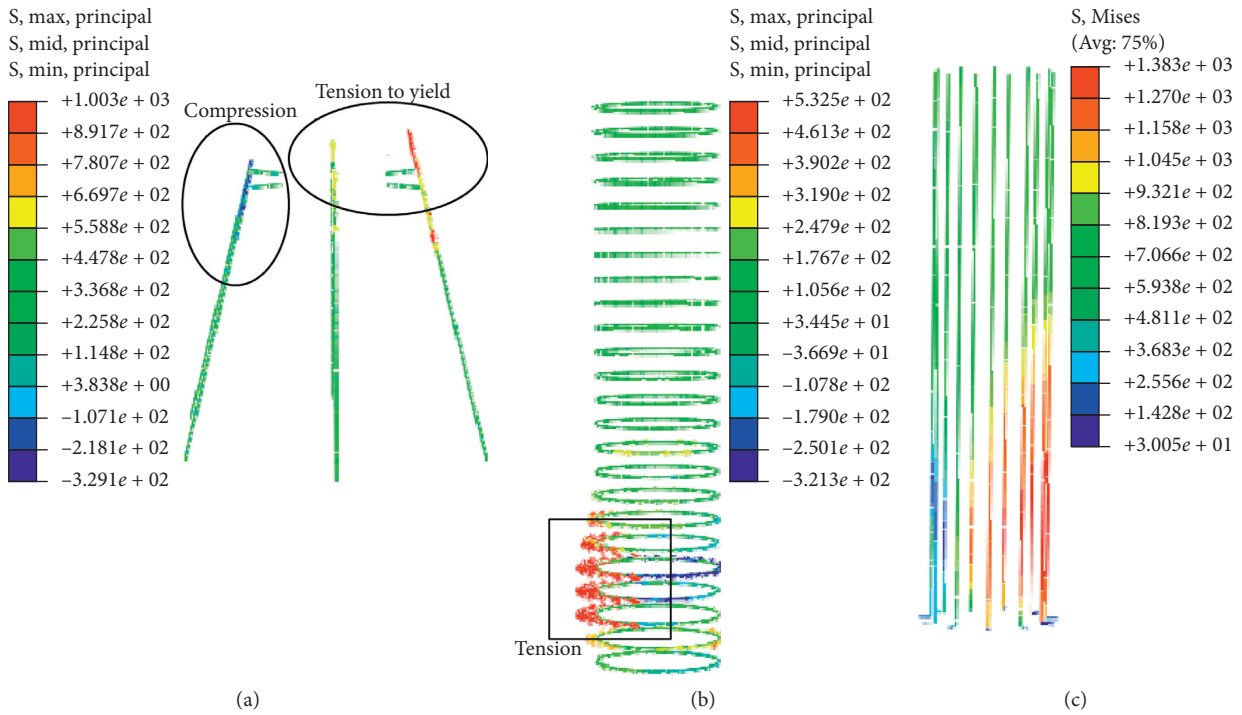

Figure 18: The stress distribution of specimen CT-9. (a) Anchor bars. (b) Stirrup. (c) Prestressed bar.

stirrup is smaller than that of specimen CT-7, and the maximum stress appears at tensile and compressive side. Figure 19(c) indicates that the maximum stress of prestressing bars is 1387 MPa due to the existence of deformed bars. Figure 19(d) indicates that the deformed bars have yielded, and the maximum stress is 496 MPa. Therefore, the tensile stress of prestressing bars decreases after the pile is reinforced with deformed bars. The connection will not fail

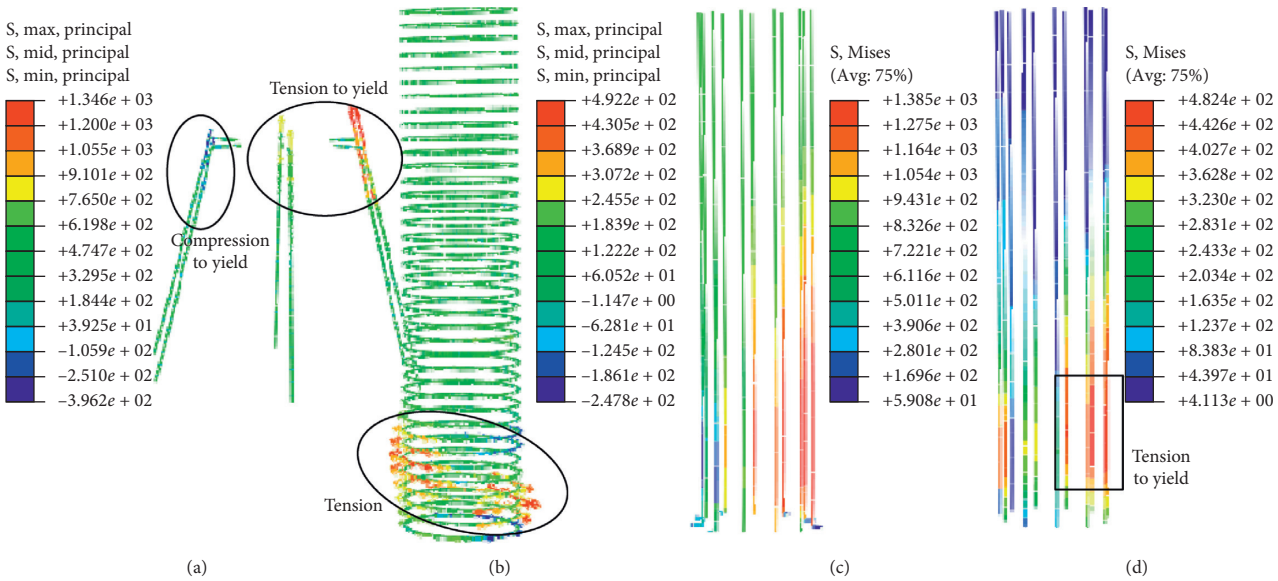

Figure 19: The stress distribution of specimen CT-10. (a) Anchor bars. (b) Stirrup. (c) Prestressed bar. (d) Deformed bars.

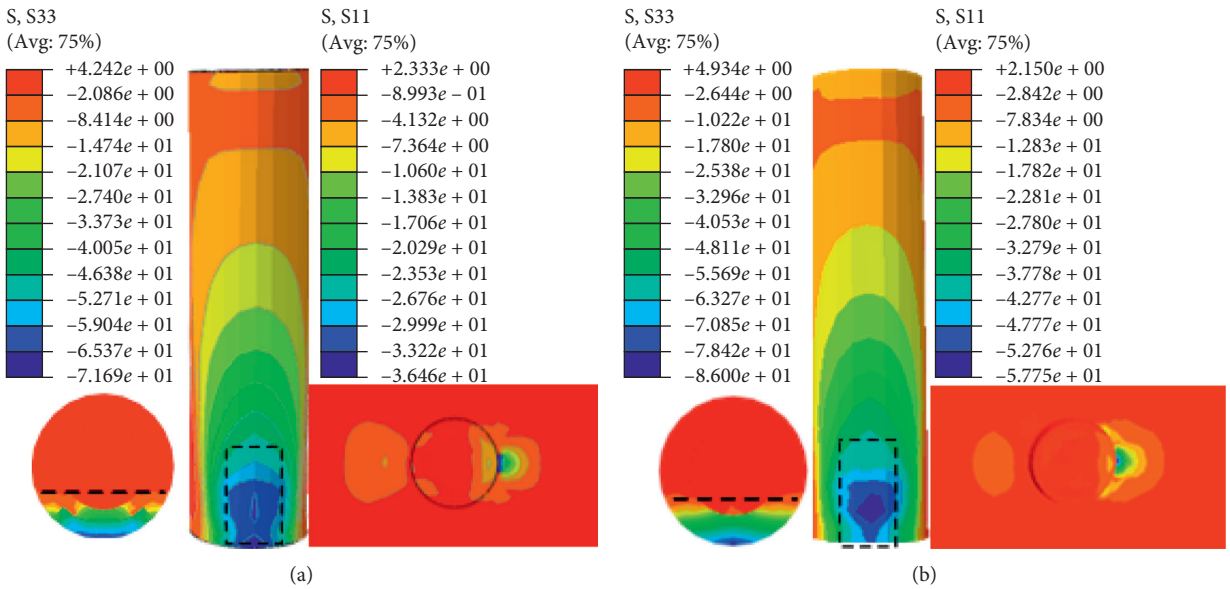

Figure 20: Continued.

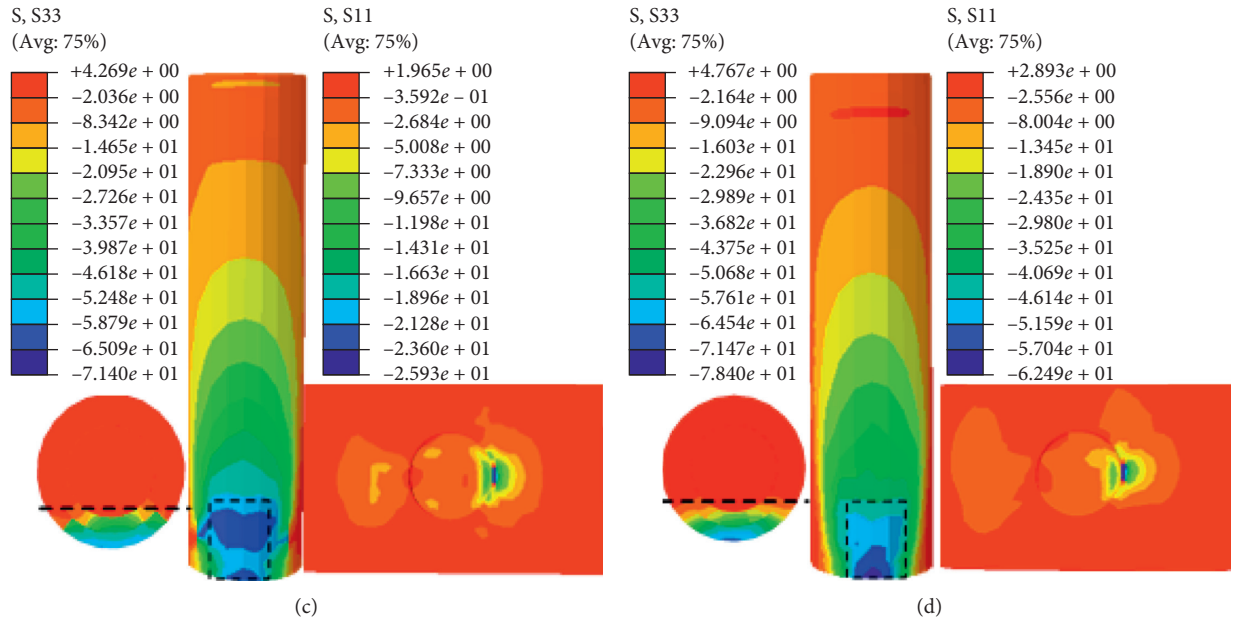

(c) (d)

Figure 20: Concrete stress distribution of CT-7~CT-10. (a) CT-7. (b) CT-8. (c) CT-9. (d) CT-10.

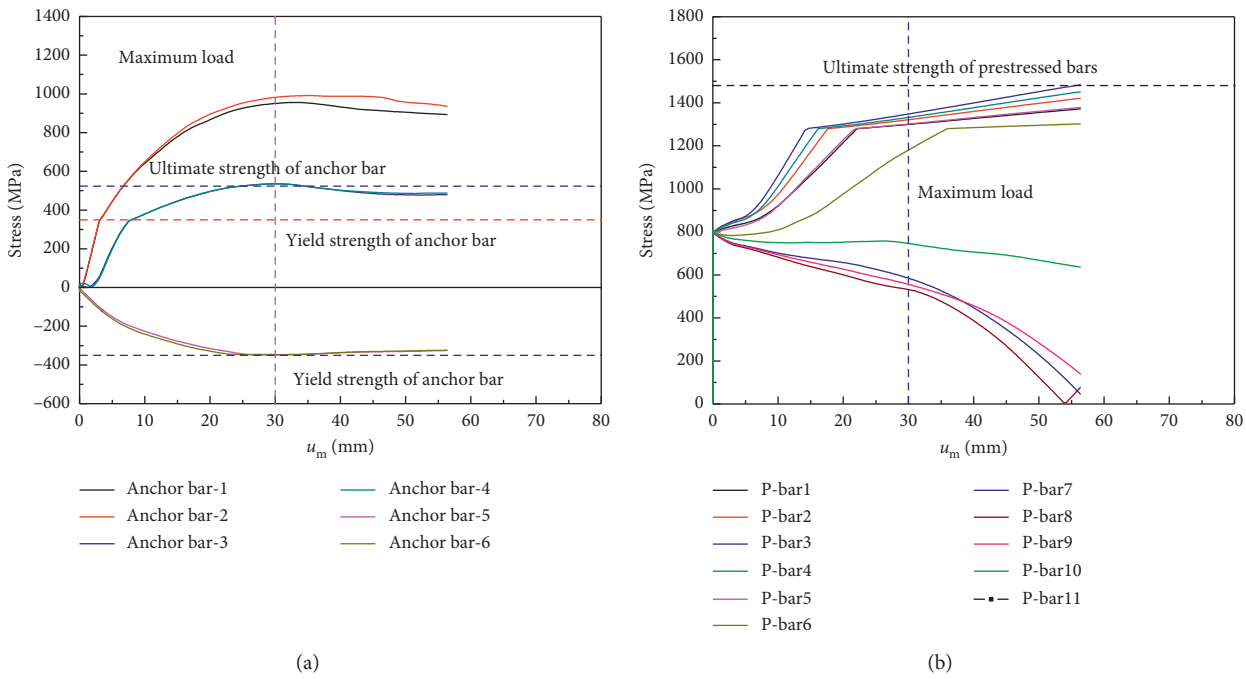

(a) (b)

Figure 21: Stress-displacement curves of CT-7. (a) Anchor bar. (b) Prestressed bar.

due to the rupture of prestressing bars, but the diameter or number of anchor bars should be increased to prevent the connection to be damaged.

5.3.2. Stress Distribution of Concrete. Figure 20 shows the concrete stress distribution of specimens CT-7~CT-10. It can be seen from Figure 20 that the concrete strength of specimen CT-8 is increased due to the confinement of CFRP. The compressive area of specimen CT-8 is bigger than that of specimen CT-7; therefore, the ultimate bearing capacity is bigger. In addition, the cap of specimen CT-8 is subjected to bigger squeezing stress than that of specimen CT-7, and the test results showed that the cap of specimen CT-8 is damaged more seriously than that of specimen CT-7.

Figure 20(c) shows that the compressive stress of pile and squeezing stress of cap is almost same with CT-7, but the maximum tensile stress is smaller than CT-7.

It can be seen from Figure 20(d) that the maximum compressive stress of pile is 78.4 MPa, and the maximum

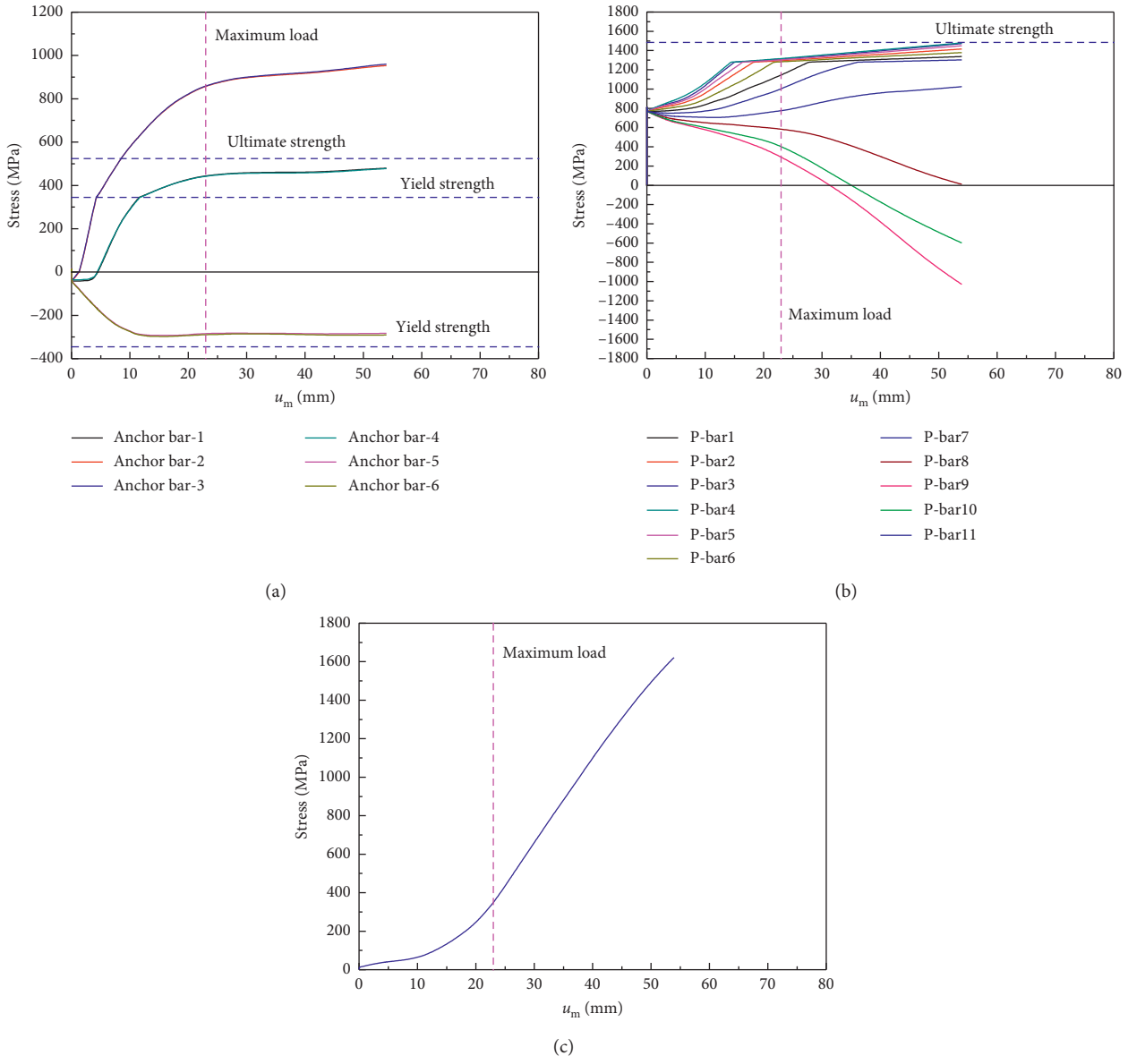

Figure 22: Stress-displacement curves of CT-8. (a) Anchor bar. (b) Prestressed bar. (c) CFRP.

squeezing stress of cap is 62.5 MPa, which is bigger than CT-7. This is because the flexural capacity of pile was reinforced by deformed bars, which caused the flexural capacity of pile cap to be increased; therefore, the compressive stress of pile and squeezing stress of cap also increased.

5.3.3. Stress-Displacement Curves of Steel Bars. The maximum stress-displacement curves of anchor bars and prestressing bars during the loading process of CT-7 are shown in Figure 21. It can be seen from Figure 21(a) that there are three different stress states for anchor bars, which is basically the same at symmetry location. All of the anchor bars at tensile zone have yielded, and the two anchor bars farthest from neutralization have reached the ultimate tensile strength.

Figure 21(b) shows that the stress of all the prestressing bars is the same before loading. The tension stress of prestressing bars in the tension zone increases with the increase of displacement. The tension stress of prestressing bars in the compressive zone decreases, and the tension stress of three prestressing bars at the maximum compressive zone is eliminated completely.

The maximum stress-displacement curves of anchor bars, prestressed bars, and CFRP during the loading process of CT-8 are shown in Figure 22. It can be seen from Figure 22 that four anchor bars were under compression at the initiation of loading. As the displacement increased, two of them gradually turned into tension and yielded at last. The two anchor bars of compressive zone did not yield because confinement of CFRP improved the flexural capacity of pile end. Compared with CT-7, the prestress of prestressing bars was eliminated more obviously, which indicates that the compression side of pile undertook greater compressive force. Figure 22(c) shows that the stress of CFRP is 326 MPa

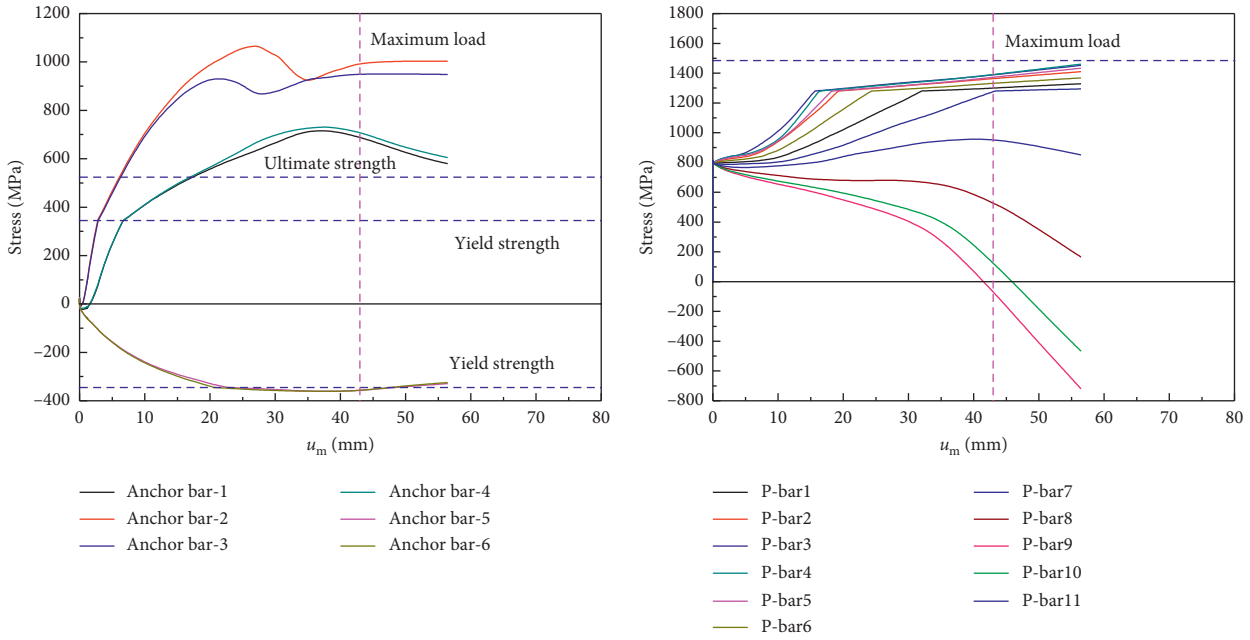

(a) (b)

Figure 23: Stress-displacement curves of CT-9. (a) Anchor bar. (b) Prestressed bar.

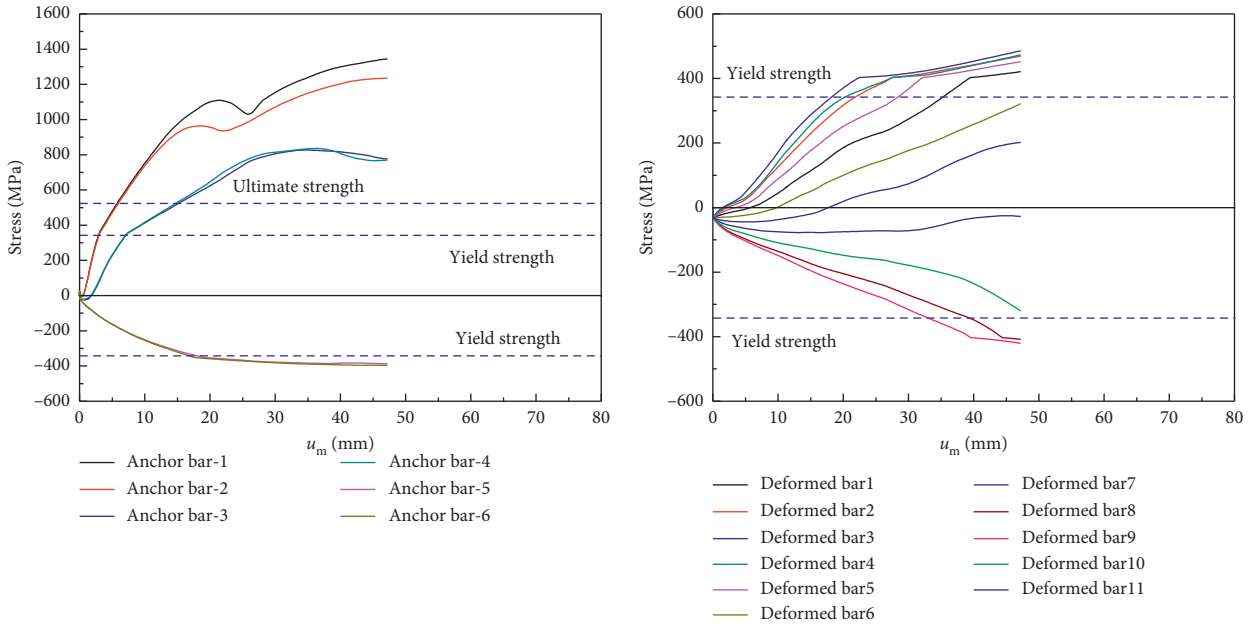

(a) (b)

Figure 24: Continued.

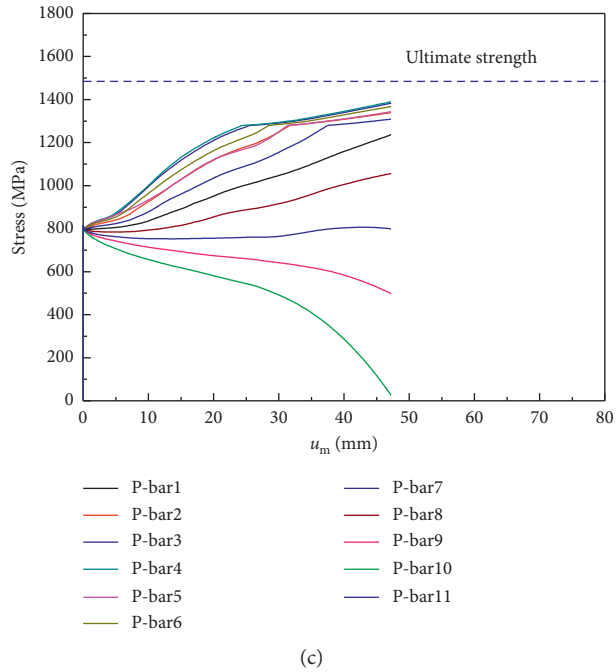

(c)

Figure 24: Stress-displacement curves of CT-10. (a) Anchor bar. (b) Deformed bar. (c) Prestressed bar.

at maximum load, and the stress increases with the increase of displacement, but it is always in the elastic stage.

The maximum stress-displacement curves of anchor bars and prestressed bars during the loading process of CT-9 are shown in Figure 23. It can be seen from Figure 23 that its stress state is similar to that of CT-7. However, the tensile stress of concrete increases due to the addition of steel fiber, which increases the flexural capacity of pile end. Therefore, its horizontal displacement is larger when researching the ultimate bearing capacity, and the tensile force of anchorage bar is larger.

The maximum stress-displacement curves of anchor bars and prestressing bars during the loading process of CT-10 are shown in Figure 24. It can be seen from Figure 24(a) that the stress of anchor bars of CT-10 is bigger than that of CT-7. Figure 24(b) indicates that the deformed bars were under compression at the initiation of loading, which is caused by prestressing stress and axial loading. With the increase of displacement, a part of deformed bars began to be tensile, and the deformed bars at maximum tensile and compression zone both yielded. Figure 24(c) shows that the tensile stress of prestressing bars decreased during the loading process of CT-10 after reinforced with deformed bars. As researching the ultimate bearing capacity, the prestressing bars did not reach their ultimate tensile strength.

It can be seen from Figures 21–24 that tensile stress of some anchor bars is larger than their ultimate strength; therefore, it is advisable to use high-strength steel bar in projects.

6. Conclusion

The following conclusions could be obtained by cyclic loading test and nonlinear finite element analysis on PHC pile to pile cap connection:

(1) The specimens were damaged due to the crushing of cap concrete in the connection area, which formed hinge joint between pile and cap and caused rotation ability of the joint to be stronger. Therefore, it is necessary to guarantee that the cap will not be damaged by the rotation of pile end too early due to the extrusion pressure and prying force.

(2) The failure region of specimens (CT-8~CT-10) mainly concentrated between pile and cap after improvement, the pile end has no severe damage, and the horizontal bearing capacity and energy dissipation performance have no significant improvement.

(3) The displacement ductility coefficient of CT-10 and CT-9 is bigger than that of CT-7, which shows that the PHC pile reinforced with steel fiber and deformed bars can improve the deformability and flexural bearing capacity of piles, which causes the displacement ductility of connection to be better.

(4) The FEA load-displacement curves are close to the experimental curves. Otherwise, there are some certain errors between the FEA and test results about the bearing capacity and stiffness, and the FEA results are not far from the test results, which can be used as a basis for further analysis. On this basis, the stress analysis of prestressing bars, deformed bars, and CFRP of ultimate state shows that the stress of prestressing bar is reduced.

Data Availability

The data used to support the findings of this study are all included in the article.

Conflicts of Interest

The authors declare that they have no conflicts of interest.

Acknowledgments

This project was supported by the National Natural Science Foundation of China (51808353), Innovative Talent Support Program for Colleges and Universities of Liaoning Province (LR2017077), and Science and Technology Innovation Talents Support Program of Shenyang (RC180270). This project was sponsored by Tianjin Poly Concrete Pile Co., Ltd., whose contribution is gratefully acknowledged. The authors thank Prof. Kang Guyi and Gu Xiaolu for their useful suggestions.

References

[1] H. Kishida., "Damage to reinforced concrete buildings in Niigata city with special reference to foundation engineering," *Soil and Foundation*, vol. 6, no. 1, pp. 71–88, 1966.

[2] K. Hideaki and T. Hanazato, "Damage of reinforced precast piles during the Miyagi-Ken-Oki earthquake of June 12, 1972," in *Proceedings of the Seventh World Conference on Earthquake Engineering, Istanbul, Turkey*, no. 6, pp. 461–468, Ankara, Turkey, 1980.

[3] M. Hatsukasu and M. Iiba, "Pile damage during the 1995 hyogoken-manbu earthquake in Japan," in *Proceedings of the 11th World Conference on Earthquake Engineering*, no. 977, pp. 383–401, Acapulco, Mexico, 1996.

[4] Y. Masatoshi, S. Joji, M. Kazuya, and M. Masaki, "Field investigation and dynamic analysis of damaged structure on pile foundation during the 2011 off the Pacific Coast of Tohoku Earthquake," in *Proceedings of the 15th World Conference on Earthquake Engineering*, no. 3195, pp. 323–332, Lisboa, Portugal, 2012.

[5] K. Tokimatsu, S. Tamura, H. Suzuki, and K. Katsumata, "Building damage associated with geotechnical problems in the 2011 tohoku pacific earthquake," *Soils and Foundations*, vol. 52, no. 5, pp. 956–974, 2012.

[6] S. Kokusho, A. Wada, K. Kobayashi, S. Mitsugi, and K. Ueda, "Experiments ON the seismic behavior OF PHC piles: study of the improvement in the bearing capacity and deformability of the prestressed high strength concrete(PHC) pile, Part 1," *Journal of Structural and Construction Engineering (Transactions of AIJ)*, vol. 376, pp. 71–80, 1987.

[7] S. Kokusho, M. Horii, A. Wada et al., "The effectiveness OF concrete fill IN the hollow part OF PHC piles: study of the improvement in the bearing capacity and deformability of the prestressed high strength concrete (PHC) pile, Part 2," *Journal of Structural and Construction Engineering (Transactions of AIJ)*, vol. 390, pp. 134–141, 1988.

[8] T. Nagae, S. Kishida, K. Katori, and S. Hayashi, "Influence of axial deformed bars and lateral reinforcement on earthquake-resistant properties of PRC piles," *Journal of Structural and Construction Engineering (Transactions of AIJ)*, vol. 65, no. 538, pp. 123–129, 2000.

[9] T. Nagae, S. Kishida, T. Yanase, K. Katori, and S. Hayashi, "Relationship between earthquake-resistant property and amount OF lateral reinforcement Of PRC pile: in case where diameter and axial load differ," *Journal of Structural and Construction Engineering (Transactions of AIJ)*, vol. 67, no. 551, pp. 95–102, 2002.

[10] M. Akiyama, S. Abe, N. Aoki, and M. Suzuki, "Flexural test of precast high-strength reinforced concrete pile prestressed with unbonded bars arranged at the center of the cross-section," *Engineering Structures*, vol. 34, pp. 259–270, 2012.

[11] J.-H. Hyun, J.-W. Bang, S.-S. Lee, and Y.-Y. Kim, "Shear strength enhancement of hollow PHC pile reinforced with infilled concrete and shear reinforcement," *Journal of the Korea Concrete Institute*, vol. 24, no. 1, pp. 71–78, 2012.

[12] J.-W. Bang, J.-H. Hyun, B.-Y. Lee, S.-S. Lee, and Y.-Y. Kim, "Flexural strength of PHC pile reinforced with infilled concrete, transverse and longitudinal reinforcements," *Journal of the Korea Concrete Institute*, vol. 25, no. 1, pp. 91–98, 2013.

[13] Z. Yang, G. Li, and W. Wang, "Experimental investigation and nonlinear finite element analysis on seismic performance of PHC piles," *Structural Engineering International*, vol. 28, no. 4, pp. 475–488, 2018.

[14] Z. Yang, G. Li, W. Wang, and Y. Lv, "Study on the flexural performance of prestressed high strength concrete pile," *KSCE Journal of Civil Engineering*, vol. 22, no. 10, pp. 4073–4082, 2018.

[15] Z. Yang, Q. Fang, B. Lv, C. Mei, and X. Fu, "An investigation into the effect of cracking on the response of drilled and postgrouted concrete pipe pile under lateral loading," *Advances in Materials Science and Engineering*, vol. 2020, pp. 1–12, 2020.

[16] P. Li, T. Zhang, and C. Wang, "Behavior of concrete-filled steel tube columns subjected to axial compression," *Advances in Materials Science and Engineering*, vol. 2018, pp. 1–15, 2018.

[17] X. Zhang, S. Niu, J.-B. Yan, and S. Zhang, "Seismic behaviour of prestressed high-strength concrete piles under combined axial compression and cyclic horizontal loads," *Advances in Structural Engineering*, vol. 22, no. 5, pp. 1089–1105, 2019.

[18] P. Wu, Y. Guo, D. Y. Zhu, W. L. Jin, Z. H. Zhang, and R. Z. Liang, "Flexural performances of prestressed high strength concrete piles reinforced with hybrid GFRP and steel bars," *Marine Georesources & Geotechnology*, vol. 38, no. 5, pp. 518–526, 2019.

[19] P. Wu, Y. Guo, D. Zhu, W. Jin, and C.-F. Lee, "Flexural performances of pre-stressed concrete piles reinforced with hybrid BFRP and steel bars," *European Journal of Environmental and Civil Engineering*, pp. 1–20, 2020.

[20] K. Wachi, S. Asano, N. Maeda, and K. Aoshima, "Mechanical characteristics of simplified connection of pile head for precast concrete pile," *Journal of Structural and Construction Engineering*, vol. 68, no. 570, pp. 85–91, 2003.

[21] K. Aoshima, H. Shimada, and T. Komuro, "Mechanical characteristics of pile head joint with improved simplified connection method for precast concrete piles," *Journal of Structural and Construction Engineering*, vol. 71, no. 607, pp. 125–132, 2006.

[22] K. Aoshima, Y. Horii, H. Kobayashi, and T. Adach, "Structural performance of improved simplified connection system at precast concrete pile head under high axial load," *Journal of Structural and Construction Engineering*, vol. 75, no. 653, pp. 1271–1278, 2010.

[23] T. Hirade, Y. Sugimura, and F. Ohsugi, "Experimental study on mechanical properties of pile headjoint for prestressed high strength concrete piles using unbonded stud bars," *Journal of Structural and Construction Engineering (Transactions of AIJ)*, vol. 69, no. 581, pp. 71–78, 2004.

[24] S. Sasaki, K. Kobayashi, H. Yamamoto, K. Kobayashi, T. Matsuyama, and Y. Utsumi, "Study on mechanical behaviour of semi-rigid connection on pile head for pre-cast concrete piles using unbonded anchors," *Journal of Structural and Construction Engineering*, vol. 72, no. 620, pp. 81–86, 2007.

[25] J.-B. Park, Y.-J. Sim, Y.-S. Chun, S.-S. Park, and Y.-B. Park, "Assessment of optimum reinforcement of rebar for joint of PHC pile and foundation plate," *LHI Journal of Land, Housing, and Urban Affairs*, vol. 1, no. 1, pp. 67–73, 2010.

[26] J. W. Bang, J. H. Hyun, B. Y. Lee, and Y. Y. Kim, "Cyclic behavior of connection between footing and concrete-infilled composite PHC pile," *Structural Engineering and Mechanics*, vol. 50, no. 6, pp. 741–754, 2014.

[27] J. W. Bang, B. Y. Lee, and Y. Y. Kim, "Flexural and shear behavior of large diameter PHC pile reinforced by rebar and infilled concrete," *Computers and Concrete*, vol. 25, no. 1, pp. 75–81, 2020.

[28] T. Wang, Z. Yang, H. Zhao, and W. Wang, "Seismic performance of prestressed high strength concrete pile to pile cap connections," *Advances in Structural Engineering*, vol. 17, no. 9, pp. 1329–1342, 2014.

[29] Z. Yang and W. Wang, "Experimental and numerical investigation on the behaviour of prestressed high strength concrete pile-to-pile cap connections," *KSCE Journal of Civil Engineering*, vol. 20, no. 5, pp. 1903–1912, 2016.

[30] Z. Guo, W. He, X. Bai, and Y. F. Chen, "Seismic performance of pile-cap connections of prestressed high-strength concrete pile with different details," *Structural Engineering International*, vol. 27, no. 4, pp. 546–557, 2017.

[31] C. A. Blandon, C. J. Krier, and J. I. Restrepo, "Behavior of full-scale prestressed pile-deck connections for wharves under cyclic loading," *Earthquakes and Structures*, vol. 16, no. 4, pp. 455–468, 2019.

[32] JGJ/94-2008, *Technical Code For Building Pile Foundation*, Architecture Industrial Press of Beijing, Beijing, China, 2008, in Chinese.

[33] C. E. Chalioris and C. G. Karayannis, "Effectiveness of the use of steel fibres on the torsional behaviour of flanged concrete beams," *Cement and Concrete Composites*, vol. 31, no. 5, pp. 331–341, 2009.

[34] C. E. Chalioris, "Analytical approach for the evaluation of minimum fibre factor required for steel fibrous concrete beams under combined shear and flexure," *Construction and Building Materials*, vol. 43, pp. 317–336, 2013.

[35] C. E. Chalioris, P. M. Kosmidou, and C. G. Karayannis, "Cyclic response of steel fiber reinforced concrete slender beams," *An Experimental Study", Materials*, vol. 12, no. 9, p. 1398, 2019.

[36] GB/T 3354-1999, *Test Method for Tensile Properties of Oriented Fiber Reinforced Plastics*, Standards Press of China, Beijing, China, 1999, in Chinese.

[37] D. J. Kakaletsis, K. N. David, and C. G. Karayannis, "Effectiveness of some conventional seismic retrofitting techniques for bare and infilled R/C frames," *Structural Engineering and Mechanics*, vol. 39, no. 4, pp. 499–520, 2011.

[38] A. G. Tsonos, "An innovative solution for strengthening of old R/C structures and for improving the FRP strengthening method," *Structural Monitoring and Maintenance*, vol. 1, no. 3, pp. 323–338, 2014.

[39] JGJ/T 101-2015, *Specification For Seismic Test of Buildings*, Architecture Industrial Press of China, Beijing, China, 2015, in Chinese.

[40] C. A. Pagni and L. N. Lowes, "Fragility functions for older reinforced concrete beam-column joints," *Earthquake Spectra*, vol. 22, no. 1, pp. 215–238, 2006.

[41] Z. H. Guo, *The Strength and Constitutive Relations of Concrete: Theory and Application*, China Building Industry Press, Beijing, China, 2003, in Chinese.